ELEMENTA
Science of the Anthropocene

Zamanillo, M, et al. 2021. Uncoupled seasonal variability of transparent exopolymer and Coomassie stainable particles in coastal Mediterranean waters: Insights into sources and driving mechanisms. *Elem Sci Anth*, 9: 1. DOI: https://doi.org/10.1525/elementa.2020.00165

RESEARCH ARTICLE

Uncoupled seasonal variability of transparent exopolymer and Coomassie stainable particles in coastal Mediterranean waters: Insights into sources and driving mechanisms

Marina Zamanillo[1,2], Eva Ortega-Retuerta[3], Carolina Cisternas-Novoa[2], Cèlia Marrasé[1], Carles Pelejero[1,4], Josep Pascual[5], Josep M. Gasol[1,6], Anja Engel[2], and Rafel Simó[1,*]

Transparent exopolymer particles (TEP) and Coomassie stainable particles (CSP) are gel-like particles, ubiquitous in the ocean, that affect important biogeochemical processes including organic carbon cycling by planktonic food webs. Despite much research on both groups of particles (especially TEP) over many years, whether they exist as distinctly stainable fractions of the same particles or as independent particles, each with different driving factors, remains unclear. To address this question, we examined the temporal dynamics of TEP and CSP over 2 complete seasonal cycles at 2 coastal sites in the Northwestern Mediterranean Sea, the Blanes Bay Microbial Observatory (BBMO) and the L'Estartit Oceanographic Station (EOS), as well as their spatial distribution along a coast-to-offshore transect. Biological, chemical, and physical variables were measured in parallel. Surface concentrations (mean $\pm$ standard deviation [*SD*]) of TEP were 36.7 $\pm$ 21.5 μg Xanthan Gum (XG) eq L^{-1} at BBMO and 36.6 $\pm$ 28.3 μg XG eq L^{-1} at EOS; for CSP, they were 11.9 $\pm$ 6.1 μg BSA eq L^{-1} at BBMO and 13.0 $\pm$ 5.9 μg BSA eq L^{-1} at EOS. Seasonal variability was more evident at EOS, where surface TEP and CSP concentrations peaked in summer and spring, respectively, and less predictable at the shore-most station, BBMO. Vertical distributions between surface and 80 m, monitored at EOS, showed highest TEP concentrations within the surface mixed layer during the stratification period, whereas CSP concentrations were highest before the onset of summer stratification. Phytoplankton were the main drivers of TEP and CSP distributions, although nutrient limitation and saturating irradiance also appeared to play important roles. The dynamics and distribution of TEP and CSP were uncoupled both in the coastal sites and along the transect, suggesting that they are different types of particles produced and consumed differently in response to environmental variability.

Keywords: Transparent exopolymer particles, Coomassie stainable particles, Mediterranean Sea, Time series, Phytoplankton

1. Introduction

The ocean, which currently absorbs ca. 30% of the anthropogenic CO_2, contains a vast amount of carbon in the form of dissolved organic matter (approximately 660 Gt; Hedges, 2002). Understanding the mechanisms that produce and recycle organic matter in the ocean is essential to predicting further changes in CO_2 capture. Marine gel-like organic particles, such as transparent exopolymer particles (TEP) and Coomassie stainable particles (CSP), have gained considerable attention in oceanography over the past years due to their involvement in biological, chemical, and physical processes such as carbon cycling, air–sea interactions, and microbial growth (Engel et al., 2020). TEP are relevant players in the carbon cycle as their production rate is estimated to represent 5%–10% of primary production in the ocean (Mari et al., 2017), and they favor the aggregation and sinking of suspended particles (Engel et al., 2004; Burd and Jackson, 2009), thus impacting the efficiency of the biological carbon pump. In addition, due to their low density (Azetsu-Scott and Passow, 2004), TEP

[1] Department of Marine Biology and Oceanography, Institut de Ciències del Mar, CSIC, Barcelona, Catalonia, Spain
[2] GEOMAR Helmholtz Centre for Ocean Research Kiel, Kiel, Germany
[3] CNRS, Sorbonne Université, UMR 7621, Laboratoire d'Océanographie Microbienne, Banyuls–sur–Mer, France
[4] ICREA, Institució Catalana de Recerca i Estudis Avançats, Barcelona, Catalonia, Spain
[5] Estació Meteorològica de L'Estartit, Girona, Catalonia, Spain
[6] Center for Marine Ecosystems Research, School of Science, Edith Cowan University, Joondalup, WA, Australia

* Corresponding author:
Email: rsimo@icm.csic.es

can ascend through the upper water column, accumulate in the sea surface microlayer (SML), and influence air–sea gas exchanges (Calleja et al., 2009; Wurl et al., 2016; Jenkinson et al., 2018). They can also be released to the atmosphere, contributing to organic aerosols (Aller et al., 2005) and impacting the Earth's radiative budget (Brooks and Thornton, 2018). Regarding CSP, there is little evidence showing a significant impact on aggregation processes (Prieto et al., 2002; Cisternas-Novoa et al., 2015), but CSP also accumulate in the SML (Wurl et al., 2011; Engel and Galgani, 2016; Zancker et al., 2017; Sun et al., 2018) and have been observed in sea spray aerosols (Kuznetsova et al., 2005; Aller et al., 2017).

Phytoplankton are the main source of TEP and presumably also of CSP in the ocean (Passow, 2002b; Thornton and Chen, 2017), although prokaryotic heterotrophs can also produce them (Stoderegger and Herndl, 1999; Radic et al., 2006). Diatoms and cyanobacteria have been shown to produce both CSP and TEP **(**Passow and Alldredge, 1994; Grossart et al., 1998; Grossart et al., 2006; Endres et al., 2013**)**. Although CSP production by other phytoplankton groups has not yet been examined (reviewed in Thornton, 2018), dissolved organic nitrogen, including protein (stained by the dye Coomassie brilliant blue [CBB]), is known to be released by phytoplankton into the surrounding medium (Hu and Smith, 1998; Suratman et al., 2008; Sarmento et al., 2013). Similarly, TEP precursors, which generally are acidic polysaccharides, are released mostly by phytoplankton (Decho, 1990) and then assembled abiotically into TEP through ionic bonding (Alldredge et al., 1993; Thornton, 2004). Such assembly is presumably also the case for CSP (Cisternas-Novoa et al., 2015), but this process has not yet been tested directly. Zooplankton (Ling and Alldredge, 2003) and prokaryotic heterotrophs (Passow, 2002a; Grossart et al., 2006; Azam and Malfatti, 2007) can use TEP, which is probably also the case for CSP (Radic et al., 2006; Endres et al., 2013; Cisternas-Novoa et al., 2015; Engel et al., 2015). Environmental and biological variables, other than the taxonomic composition of phytoplankton and prokaryotic heterotrophs, impact the production of TEP in the ocean. Phytoplankton physiological state (Passow, 2002a), temperature (Claquin et al., 2008), light intensity (Trabelsi et al., 2008), and nutrient availability (Radic et al., 2006) may alter the production of TEP, while losses can occur through UV-induced photolysis (Ortega-Retuerta et al., 2009). Owing to the lack of similar studies with CSP, only nutrient availability is known to affect CSP production (Radic et al., 2006), while physiological stress did not enhance CSP production by diatoms and cyanobacteria in culture (Thornton and Chen, 2017).

TEP and CSP are defined by the specific dyes that stain them: TEP by Alcian Blue, which stains acidic polysaccharides (Alldredge et al., 1993; Passow and Alldredge, 1995), and CSP by CBB, which stains proteins (Long and Azam, 1996; Engel, 2009). CSP are thought to contain 5–7 times more nitrogen than TEP (Engel and Passow, 2001; Mari et al., 2001), although their content has not been measured directly. TEP have been thoroughly studied in the ocean (reviewed by Passow, 2002b, Bar-Zeev et al., 2015, and Mari et al., 2017). Conversely, CSP were rarely described until the recent development of a spectrophotometric method (reviewed by Thornton, 2018), which is less time-consuming and labor-intensive than the classical microscopic quantification (Cisternas-Novoa et al., 2014).

Our knowledge of the temporal dynamics of CSP remains limited to a handful of studies at sites where TEP and CSP were measured in parallel. One of these studies was conducted in a low-salinity temperate coastal site in the Baltic Sea, where CSP concentration, measured in both the SML and the subsurface water (SSW), increased in summer and was generally similar to that of TEP (Dreshchinskii and Engel, 2017). In studies in the Sargasso Sea (Cisternas-Novoa et al., 2015) and the Fram Strait (von Jackowski et al., 2020), TEP and CSP presented different temporal and vertical distributions. The 2 particle types were also temporally uncoupled during the course of a phytoplankton bloom in a mesocosm study (Cisternas-Novoa et al., 2015).

The northwestern (NW) Mediterranean Sea is a temperate oligotrophic sea, characterized by the enhancement of water stratification in late spring and summer due to the increase in solar radiation, which leads to low nutrient concentrations in surface waters (Sala et al., 2002; Duarte et al., 2004; Lucea et al., 2005) and minimum chlorophyll *a* (Chl*a*) concentrations, and by vertical mixing in fall through winter. Chl*a* concentration in the NW Mediterranean Sea is usually highest in late winter or early spring, triggered by the onset of thermal stratification after winter mixing, coinciding with nutrient availability and high solar radiation (Marty et al., 2002; Gasol et al., 2016). However, the specific conditions that prompt the onset of the bloom in the Mediterranean Sea and other regions are still under debate (Smetacek and Cloern, 2008; Behrenfeld, 2010; Taylor and Ferrari, 2011).

Previous studies of the temporal dynamics of TEP in the Mediterranean Sea, other than those conducted in eutrophic coastal areas or zones heavily influenced by the presence of seagrass meadows (Radic et al., 2005; Scoullos et al., 2006; Iuculano et al., 2017a), showed maximum TEP concentrations in summer, both at coastal and offshore sites (Beauvais et al., 2003; Ortega-Retuerta et al., 2018), with a temporal mismatch between TEP and Chl*a* (Ortega-Retuerta et al., 2018). In contrast, there are no published studies of CSP distributions in the Mediterranean Sea.

This study was motivated by the paucity of empirical studies on the distribution and seasonality of CSP and their relationship with those of TEP (Cisternas-Novoa et al., 2015; Thornton et al., 2016; Thornton and Chen, 2017; Thornton, 2018). Our main objective was to elucidate whether or not these 2 pools of organic particles follow similar trends over the year and across horizontal and vertical scales. Based on a previous study (Cisternas-Novoa et al., 2015), we hypothesized that CSP distributions and their temporal dynamics would be closely related to those of phytoplankton biomass, while TEP distribution and dynamics would be related to the combination of phytoplankton biomass and taxonomic composition, solar radiation, and nutrient limitation. To test these hypotheses, we assessed the temporal dynamics

of TEP and CSP simultaneously over 2 complete seasonal cycles at 2 coastal sites of the NW Mediterranean Sea characterized by strong seasonality. At the shore-most site, the Blanes Bay Microbial Observatory (BBMO), we followed TEP and CSP concentrations near the surface; at the offshore site, the L'Estartit Oceanographic Station (EOS), which presents a conspicuous deep chlorophyll maximum (DCM) between 20 and 80 m, we examined the seasonal variations in the vertical distribution of TEP and CSP. Horizontal variations of TEP and CSP were also analyzed at 2 depths in a nearby coast-to-offshore transect.

2. Material and methods

2.1. Study sites and sampling

Samples were collected within the Catalan Sea of the NW Mediterranean at (1) the BBMO site at 41.40°N, 2.48°E (http://bbmo.icm.csic.es); (2) the EOS site, 70 km further north at 42.05°N, 3.25°E, and (3) stations along a transect between the Catalan Coast near BBMO and Mallorca Island, on board the RV *García del Cid* for a cruise designated MIFASOL II (**Figure 1**). The BBMO is located around 800 m offshore, in an open bay with shallow waters (sandy bottom at 20 m depth) that only weakly stratifies in summer and where most terrestrial inputs arrive as runoff from the surrounding coastal area (details in Guadayol et al., 2009a, and Gasol et al., 2012). The EOS is located 3.2 km off the main coast and 2 km off the Medes Islands, over a water column approximately 92 m deep (**Figure 1**) that strongly stratifies in summer and is heavily influenced by wind dynamics (Aparicio et al., 2017).

The BBMO and EOS samplings were performed at least once per month, from June solstice 2015 to October 2017, except during adverse weather conditions. At BBMO, water samples were taken with an acid-cleaned bucket from the surface, prefiltered through an acid-cleaned 200-µm mesh net to remove large plankton and kept in 20-L acid-cleaned polycarbonate carboys. Carboys were maintained under dim light, covered with black plastic bags to avoid light interference. Further processing of samples was done within 1.5 h at the laboratory. At EOS, 4 depths (surface, 20, 50, and 80 m) were sampled using 5-L Niskin bottles and then filtered through an acid-cleaned 200-µm nylon mesh. Water for TEP and CSP analyses was collected in 1-L acid-cleaned polycarbonate bottles, while those for the rest of variables were kept in 8-L acid-cleaned polyethylene carboys, all of them covered with black plastic bags. Polycarbonate bottles were transported in a cooler box with pack ice. Sample processing was done at the home laboratory within 4 h.

The coast-to-offshore transect was conducted during the MIFASOL II cruise, from October 22, 2015, to October 24, 2015, reaching 145 km from shore, and including stations on the shelf (station 1, closest to the shore), continental slope (stations 2–4), and deep basin (stations 5–7). Seawater was collected at 2 depths: the surface (5 m) and, when present, the DCM, using Niskin bottles (12 L) on a 12-bottle rosette with conductivity–temperature–depth (CTD) casts. Surface variables measured during the transect were TEP, CSP, Chl*a*, inorganic nutrients, prokaryotic heterotroph abundance, and picophytoplankton abundance (flow cytometry). At the DCM, only TEP, CSP, and Chl*a* were measured.

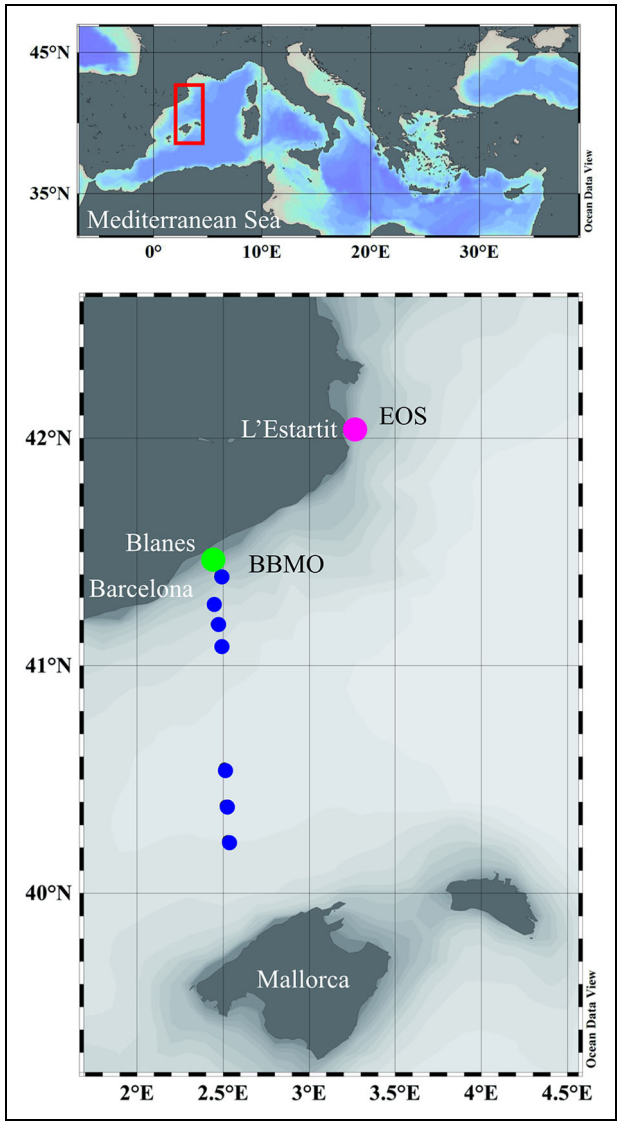

Figure 1. Map of the study area. The Blanes Bay Microbial Observatory (green circle), L'Estartit Oceanographic Station (pink circle), and the transect between the Catalan Coast and Mallorca Island (blue circles). DOI: https://doi.org/10.1525/elementa.2020.00165.f1

2.2. Physical variables

A calibrated SAIVA/S SD204 sensor was used to measure vertical profiles of temperature and salinity at BBMO and EOS. In August 2016, at BBMO and from May to June 2016 at EOS, the sensor was inoperative. We calculated the mixed layer depth (MLD) as the depth where temperature changed more than 0.15°C with respect to a reference depth of 1 m. At BBMO, we calculated a stratification index that we defined as the temperature difference between the surface and near the sea bottom (20 m). At EOS, the stratification index was defined as the temperature difference between the surface and just below the thermocline. Water transparency (in meters) was measured

with a Secchi disk at the BBMO and with white-faced Niskin bottles (used as analogous to a Secchi disk) at the EOS. The light extinction coefficient (K_d, m^{-1}) was calculated as 1.7/water transparency (Kirk, 1994). Total irradiance at 2 m was recorded hourly by a pyranometer at the Malgrat de Mar station, situated at 41° 38′ 57″N, 2° 45′ 8″E, 520 m from the coast (approximately 5 km southwest of BBMO) and the Sant Pere Pescador station (approximately 25 km north of EOS; Catalan Meteorological Service, www.meteo.cat). We measured the average solar radiation of the 24 h previous to the sampling and calculated the daily-averaged solar radiation dose as:

$$\text{Solar radiation dose} = \frac{I}{K_d \times \text{MLD}} \times (1 - e^{(-K_d \times \text{MLD})}),$$

where I is the average surface irradiance (W m^{-2}) in the 24 h previous to sampling, K_d is the light extinction coefficient (m^{-1}), and MLD is the mixed layer depth (m).

During the MIFASOL II cruise, a SBE21 Sea Cat Thermosalinograph was used to obtain surface temperature and salinity and a CTD SBE911 plus to record vertical profiles down to 400 m.

2.3. Chemical and biological variables

2.3.1. Particulate organic matter (TEP, CSP, particulate organic carbon [POC], and particulate organic nitrogen [PON])

TEP were analyzed following the spectrophotometric method proposed by Passow and Alldredge (1995). Samples (150–500 mL) were filtered in duplicate under constant low pressure (approximately 150 mm Hg) onto 25-mm diameter 0.4-μm pore size polycarbonate filters (DHI Lab, Denmark). Immediately, the filters were stained with an Alcian Blue solution (500 μL, 0.02%, pH 2.5) for 5 s and rinsed with Milli-Q water. All sampling material was prewashed with HCl (10%) and Milli-Q water, and the first milliliters of sample were discarded. All filters remained frozen until further processing. Filters were soaked in 5 mL of 80% sulphuric acid for 3 h, shaking them intermittently, and absorbance of the solution was measured with the spectrophotometer at 787 nm (Varian Cary 100 Bio). The absorption of every batch of Alcian Blue was calibrated using an XG solution that was homogenized with a tissue grinder and measured by weight difference. A total of 7 calibrations of different Alcian Blue solutions were carried out during the temporal series. Calibration factors ranged from 123 to 231 μg XG eq A^{-1} (average ± *SD* of 171 ± 38 μg XG eq A^{-1}, where eq refers to equivalents and A is absorbance) and detection limits ranged from 0.021 to 0.048 absorbance units. Duplicate blanks (empty filters stained with Alcian Blue) were also prepared with every batch of filtered samples. TEP values are reported as the average of analytical duplicates in units of μg XG eq L^{-1}. We conducted TEP analyses in formalin-fixed (1% final concentration) samples, which were preserved at 4°C until filtration (within 4 months at most). We decided to conduct TEP analyses on fixed samples, since formalin does not interfere with the measurement (Passow and Alldredge, 1995; Ortega-Retuerta et al., 2018), and in order to optimize the number of samples processed every time a new calibration curve was obtained (1 every 4 months). To estimate TEP carbon content (TEP-C), we used the conversion factor of 0.51 μg TEP-C μg XG eq^{-1} (Engel and Passow, 2001).

CSP concentration was determined by spectrophotometry following Cisternas-Novoa et al. (2014). Duplicate samples (200–350 mL) were filtered onto 25-mm diameter 0.4-μm pore size polycarbonate filters (Whatman and DHI) using a constant low filtration pressure (approximately 150 mmHg). The samples were stained immediately with 1 mL of CBB-G 250 solution (0.04%, pH 7.4) for 30 s, always prepared with the same filtered (0.2 μm) seawater from Medes, 80 m depth, and rinsed with Milli-Q water 3 times. The filters were stored frozen in 15-mL polypropylene tubes until further processing in the laboratory (within 4 months). Duplicate blanks (stained empty filters) were prepared with every batch of filtered samples. Both the sample and blank filters were soaked in 4 mL of extraction solution (3% sodium dodecyl sulfate in 50% isopropyl alcohol), and the tubes were incubated in a water bath for 2 h at 37°C. The filters were shaken every 30 min during this period. Optimal water bath temperature and shaking conditions were determined prior to analyzing the samples. We avoided sonication as DHI filters do not withstand sonication. We used Whatman Nuclepore filters (apt for sonication) to test that the water bath and shaking were enough to remove the stain from the filters. We measured the absorbance after extraction in the water bath for 2 h and then sonicated the same filters for 2 h and measured the absorbance again. More than 90% of absorbance was recovered without sonication in our samples. The samples were then measured spectrophotometrically at 615 nm (Varian Cary 100 Bio and Shimadzu UV–Vis spectrophotometer UV120). Concentrations of CSP, reported as averages of duplicate measurements, were determined relative to a bovine serum albumin standard and expressed in units of μg BSA eq L^{-1} after Cisternas-Novoa et al. (2014). A total of 3 calibrations of different CBB solutions were carried out during the temporal series, with calibration factors ranging from 51 to 111 μg BSA eq A^{-1} (average of 73 ± 33 μg BSA eq A^{-1}), and detection limits ranged from 0.0440 to 0.0609 absorbance units.

In 4 of the BBMO samplings (November 2016 and April, August, and October 2017), TEP and CSP were also measured following the microscopy method (Alldredge et al., 1993; Passow and Alldredge, 1995). Duplicate samples of 50 mL were filtered onto 25-mm diameter 0.4-μm pore size polycarbonate filters (DHI), stained, and the excess dye removed. Blanks were prepared as stained empty filters. The filters were placed on the white side of a semitransparent glass slide (CytoClear, Poretics Corp., Livermore, US) and stored frozen (–20°C) until microscopic analysis. Following Engel (2009), abundance, area, and size–frequency distribution of TEP and CSP in the size range of 1–760 μm were determined using a light microscope (Olympus Bx61) connected to a camera (Olympus DP72). Filters were screened at 200× magnification. Thirty pictures were taken randomly from each filter along 2 perpendicular cross sections (15 pictures each; resolution 1,360 × 1,024 pixel, 8-bit color depth). ImageJ image

analysis software (version 1.44, public domain, developed at the U.S. National Institutes of Health) was used to semi-automatically analyze particle numbers and area.

For POC and PON analyses, seawater (1,000 mL) was filtered through combusted (4 h, 450°C) GF/F glass fiber filters (Whatman) and filters frozen at –20°C until processed. Prior to analysis, the filters were thawed in an HCl-saturated atmosphere for 24 h to remove inorganic compounds. The filters were then dried and analyzed with an elemental analyzer (Perkin-Elmer 2400 CHN). No replicates were collected due to water volume limitations.

2.3.2. Chl*a*

Chl*a* measurements started by filtering 150 mL (BBMO) or 100 mL (EOS) of seawater on GF/F filters (Whatman, 25-mm diameter) and storing filters at –20°C until further processing. The pigment was extracted in acetone (90% v:v) at 4°C in the dark for 24 h. Fluorescence was measured with a calibrated Turner Designs fluorometer, following Yentsch and Menzel (1963). Analytical duplicates were taken, with average coefficient of variation between duplicates of 3%.

2.3.3. Inorganic nutrients

Dissolved inorganic nutrients (nitrate, phosphate, and silicate) were measured with standard segmented flow analysis with colorimetric detection (Hansen and Grasshoff, 1983), using a SEAL Auto Analyzer AA3 HR (BBMO) or Bran + Luebe autoanalyser (EOS).

2.3.4. Phytoplankton identification and biomass

Phytoplankton > 5 μm were identified and counted with an inverted microscope. Seawater was fixed with hexamine-buffered formaldehyde solution (4% final concentration) and 100 mL were allowed to settle in Utermöhl chambers at 4°C until analysis (Utermöhl, 1958). The samples were stored for a maximum of 6 months, and we did not observe any signs of cell damage. Phytoplankton was identified to the species level when possible and finally classified into 4 groups: diatoms, dinoflagellates, coccolithophores, and "other microalgae." We used conversion equations to calculate cell C content from volume measurements (Menden-Deuer and Lessard, 2000). For diatoms, we used log pg C cell^{-1} = log –0.541 (0.099) + 0.811 (0.028) × log *V*; for the other algae groups, log pg C cell^{-1} = log –0.665 (0.132) + 0.939 (0.041) × log *V*, where *V* is cell volume in μm^3 and the values inside parentheses are the 95% confidence intervals.

2.3.5. Picophytoplankton, nanophytoplankton, and prokaryotic heterotroph abundance and biomass

Picophytoplankton (*Prochlorococcus*, *Synechococcus*, and picoeukaryotes), nanophytoplankton (photosynthetic nanoeukaryotes), and heterotrophic prokaryotes were enumerated by flow cytometry after fixation with 1% paraformaldehyde plus 0.05% glutaraldehyde (final concentrations), following standard methods (Gasol and Morán, 2015). Abundances were converted to biomass (μg L^{-1}) using average C-to-cell conversion factors gathered in Simó et al. (2009) of 51 ± 18 fg C cell^{-1} for *Prochlorococcus* (22 source studies), 175 ± 73 fg C cell^{-1} for *Synechococcus* (28 source studies), 1,319 ± 813 fg C cell^{-1} for picoeukaryotes (24 source studies), and fg C cell^{-1} = 220 V (μm^3) for photosynthetic nanoeukaryotes (1 source study), where cell volume *V* was set to 34 μm^3 (assuming a spherical model with a radius of 2 μm). The carbon content of prokaryotic heterotrophs was estimated empirically from the bead-standardized side scatter of the relevant populations following Calvo-Díaz and Morán (2006). Size was converted to C content following Norland (1993), yielding the estimated average biomass per cell in our study of 19.0 ± 0.5 fg C (n = 30) at BBMO and 19.3 ± 2.7 fg C (n = 19) at EOS.

2.4. Statistical analyses

The nonparametric Wilcoxon–Mann–Whitney test was used to check for statistical differences in the different environmental variables among seasons. The seasons were separated by the winter/summer solstices and the spring/fall equinoxes. We also used the nonparametric Wilcoxon–Mann–Whitney test to assess statistical differences of the variables among regions (BBMO and EOS). We performed pairwise Spearman correlation analyses to test for covariations between environmental and biological variables in the BBMO, EOS, and MIFASOL II data sets. Bivariate analyses (ordinary least squares) between TEP and CSP concentrations and several biological, chemical, and physical variables were performed in EOS profiles. We log-transformed data to fulfill the requirements of parametric tests. A harmonic analysis of the annual component (period, 365 days) of the TEP and CSP time series was performed using the *HarmonicRegression* package in the R software (Lueck et al., 2015). The samplings of December 2016 were not used in the harmonic analysis because these anomalously high TEP and CSP values were thought to be a response to freshwater discharges. Statistical tests, calculations, and illustrations were performed with Microsoft Office Excel 2010, Ocean Data View software version 4 (Schlitzer, 2017), and R (version 3.5.1).

SD (σ) was calculated using the following formula:

$$\sigma = \sqrt{\frac{\sum (x - \bar{x})^2}{(n-1)}},$$

where $\bar{x}$ is the mean of the sample and n is the sample number.

Standard error (*SE*) was calculated as:

$$SE = \frac{\sigma}{\sqrt{n}}.$$

3. Results

3.1. Variation of the main physical and chemical variables in the time series

BBMO and EOS are 2 sites relatively unaffected by human impacts or river discharges (Guadayol et al., 2009a; Ros and Gili, 2015), where oceanographic variables present the typical seasonal cycle of temperate coastal systems. SST changed from an average ± *SD* of 13.4°C ± 0.4°C (BBMO) and 13.2°C ± 0.5°C (EOS) in winter to 22.9°C ± 2.2°C

(BBMO) and 22.6°C ± 1.4°C (EOS) in summer (**Table 1**, Figures S1 and S2). In summer, high heat fluxes led to higher surface temperatures and the development of a shallow stratified layer (average MLD of 6.5 ± 5.7 m in BBMO and 4.6 ± 4.7 m in EOS; **Table 1**). Water transparency ranged from 5 to 20 m in BBMO and 5 to 24 m in EOS, with the highest values in summer at both stations. Dissolved nitrate and silicate concentrations in the surface were lowest in summer at both BBMO and EOS (**Table 1**). However, surface phosphate concentrations (average of 0.04 ± 0.02 μmol L^{-1} in BBMO and 0.04 ± 0.06 μmol L^{-1} in EOS) did not exhibit marked seasonal variations but were low throughout the year at both stations (**Table 1**). Dissolved inorganic nutrients at EOS usually increased with depth in summer months, while they were homogeneously distributed across depth in the other seasons, with a few exceptions (Figure S3).

3.2. Variation of TEP, CSP, POC, and PON over the time series

The ranges and averages of surface TEP concentrations were similar at both coastal stations. At BBMO, surface TEP concentrations ranged from 8.4 to 80.9 μg XG eq L^{-1} (average ± *SD* of 36.7 ± 21.5 μg XG eq L^{-1}; **Figure 2**), while at EOS, they ranged from 5.8 to 126 μg XG eq L^{-1}, with an average of 36.6 ± 28.3 μg XG eq L^{-1} (**Table 1**, **Figure 3**). Regarding seasonal patterns in surface waters, higher TEP concentrations were observed recurrently in early summer (**Figures 2** and **3**), which was confirmed by harmonic analyses for both BBMO ($P = 0.03$) and EOS ($P = 0.04$; Figure S4). The exception to this general pattern was the sample from December 2016, when a peak of TEP concentration at the surface coincided with a sharp decrease in salinity at both stations. At BBMO, this salinity drop was accompanied with higher nitrate and Chl*a* concentrations; at EOS, it came along with an increase in phosphate (Figures S1 and S2).

The higher concentration of TEP at EOS was observed between the surface and 20 m in summer, coinciding with shallow mixed layers, while TEP concentration was usually homogeneously distributed during the rest of the year, despite the presence of a mixed layer in certain months (April, May, September, and October 2017).

CSP concentrations in the surface waters were similar at both stations (**Table 1**). In BBMO, surface CSP concentration varied between 4.7 and 24.8 μg BSA eq L^{-1} (average ± *SD* of 11.9 ± 6.1 μg BSA eq L^{-1}; **Figure 2**), while at EOS, it varied between 4.5 and 22.4 μg BSA eq L^{-1} (average of 13.0 ± 5.9 μg BSA eq L^{-1}; **Figure 3**). CSP concentrations only followed a significant seasonal pattern at EOS (harmonic analysis, $P = 0.02$). Differences in vertical CSP distributions also occurred among seasons at EOS (Figure S3). In summer, CSP concentrations were higher at 20 m, that is, below the mixed layer depth. In spring, concentrations were higher within the mixed layer depth, although in April and May 2017, a peak was also observed at 60 m. In fall and winter, there was no clear pattern of CSP distribution with depth (Figure S3).

POC and PON concentrations were also similar in both coastal stations (**Table 1**), but no clear seasonal patterns were detected (harmonic analysis, $P > 0.05$). At BBMO, surface POC ranged from 5.82 to 33.16 μmol L^{-1} (average ± *SD* of 12.1 ± 6.0 μmol L^{-1}; **Figure 2**); at EOS, it ranged from 4.33 to 18.02 μmol L^{-1} (average of 9.9 ± 4.1 μmol L^{-1}; **Figure 3**). Surface PON concentrations averaged 1.8 ± 1.0 μmol L^{-1} at BBMO and 1.5 ± 1.7 μmol L^{-1} at EOS. At both BBMO and EOS, TEP and POC dynamics were significantly correlated ($r = 0.41$, $P = 0.028$, $n = 29$ at BBMO and $r = 0.50$, $P = 0.029$, $n = 19$ at EOS; **Table 2**). CSP was significantly correlated to POC ($r = 0.58$, $P = 0.021$, $n = 16$) and PON ($r = 0.57$, $P = 0.020$, $n = 16$) only at EOS. TEP and CSP were not correlated at any of the stations ($P > 0.05$; **Table 2**).

3.3. TEP and CSP size distributions

The TEP size distributions, determined by microscopy and image analysis in surface waters of BBMO in 4 different months (November 2016 and April, August and October 2017), followed an exponential distribution, with the smallest particles (<1.25 μm), being the most abundant in 3 of the 4 samples. In April 2017, a unimodal distribution was observed, with particles ranging from 2.5 to 3.5 μm being the most abundant, followed by the smallest ones (**Figure 4**). The slopes of the linear regressions between average particle diameter and TEP abundance (log-transformed) were −1.53, −1.83, −1.84, and −0.93 for November, April, August, and October, respectively.

The CSP size distributions followed an exponential shape with higher abundances of the smaller particles in the 4 samples analyzed (**Figure 4**). The slopes of the linear regressions between average particle diameter and TEP abundance (log-transformed) were −1.34, −1.42, −1.52, and −1.34 for November, April, August, and October, respectively.

3.4. Variation of biological variables over the time series

Chl*a* concentrations were similar at both stations (**Table 1**), varying between 0.13 and 1.52 μg L^{-1} (average ± *SD* of 0.49 ± 0.39 μg L^{-1}) in the surface of BBMO (**Figure 2**), between 0.13 and 0.75 μg L^{-1} (average of 0.31 ± 0.19 μg L^{-1}) in the surface of EOS (**Figure 3**), and between 0.05 and 0.84 μg L^{-1} (average of 0.34 ± 0.19 μg L^{-1}) in the whole water column of EOS (Figure S3). Maximum concentrations occurred in winter at both stations (**Table 1**). Total phytoplankton biomass (Figure S3) was not correlated with Chl*a* at either of the 2 stations ($P > 0.05$) and was maximum in late winter in both cases. Prokaryotic heterotroph abundance at the surface ranged from 5×10^5 to 17.26×10^5 cells mL^{-1} at BBMO (**Figure 2**) and from 6.69×10^4 to 6.90×10^5 cells mL^{-1} at EOS (**Figure 3**).

Phytoplankton communities were similar at both stations (Figures S1 and S2). Highest surface abundances of *Prochlorococcus* cells generally occurred in fall (except at EOS in 2016, where *Prochlorococcus* was found in spring), whereas maxima of *Synechococcus* occurred in spring. Picoeukaryotes and nanoeukaryotes were generally more abundant during the first 4 months of each year. The highest diatom biomasses were found in late fall.

Table 1. Averages ± standard deviation of the main physical and biological variables in the sea surface for each season at the BBMO and EOS time series, between June 2015 and November 2017. DOI: https://doi.org/10.1525/elementa.2020.00165.t1

	BBMO[b]				EOS[b]			
Variable[a]	Winter ($n = 6$)[c]	Spring ($n = 6$)	Summer ($n = 11$)	Fall ($n = 7$)	Winter ($n = 5$)	Spring ($n = 4$)	Summer ($n = 6$)	Fall ($n = 6$)
Temperature (°C)	13.4 ± 0.4^{A}	16.8 ± 3.0$^{B, C}$	22.9 ± 2.2^{D}	17.9 ± 2.7^{C}	13.2 ± 0.5^{A}	15.7 ± 1.7$^{B, C}$	22.6 ± 1.4^{D}	17.2 ± 1.8^{C}
Salinity	38.2 ± 0.1^{A}	38.1 ± 0.1$^{B. D}$	37.9 ±0.1$^{B, C}$ (10)	37.9 ± 0.7$^{A, D}$	38.0 ± 0.4^{A}	37.8 ± 0.3$^{A, B}$ (3)	37.8 ± 0.2^{B}	37.9 ± 0.4^{b}
Stratification index (°C)	0.04 ± 0.06$^{A, C}$	1.24 ± 1.35$^{B, C}$	2.01 ± 1.73^{B}(10)	0.49 ± 1.63$^{C, A}$	–0.15 ± 0.38$^{A, C}$	8.70 ± 8.19$^{B, C}$	10.18 ± 5.98^{B}	2.08 ± 2.10$^{a, c}$
Water transparency (m)	11.0 ± 4.0^{A}	16.5 ± 3.1$^{A, C}$	17.5 ± 3.0$^{B, C}$	15.3 ± 3.5$^{B, C}$	11.2 ± 2.9^{A}	12.8 ± 3.6$^{A, B}$	17.7 ± 3.5^{B}	14.2 ± 6.7$^{a, b}$
MLD (m)	18.0 ± 3.2^{A}	8.6 ± 6.8$^{B, C}$	6.5 ± 5.7^{C} (10)	13.9 ± 5.4$^{A, B}$	80.2 ± 28.7^{A}	6.0 ± 5.7$^{A, B}$ (2)	4.6 ± 4.7^{B} (5)	52.2 ± 38.8^{b}
Solar radiation dose (Wm^{-2})	40.2 ± 25.7^{C}	179 ± 103$^{A, B}$	220 ± 72^{B} (10)	61.1 ± 30.8$^{A, C}$	10.8 ± 5.7^{A} (4)	221 ± 99.5$^{A, B}$ (2)	235 ± 80.6^{B} (5)	36.9 ± 56.6^{b}
Nitrate (μmol L^{-1})	0.89 ± 0.47^{A}	0.34 ± 0.29$^{A, B}$	0.22 ± 0.18^{B}	0.68 ± 0.65^{B}	1.67 ± 0.20^{A} (4)	0.77 ± 0.58$^{A, B}$	0.27 ± 0.41^{B}	1.36 ± 1.23^{b}
Phosphate (μmol L^{-1})	0.06 ± 0.04^{A}	0.03 ± 0.01^{A}	0.04 ± 0.02^{A}	0.04 ± 0.01^{A}	0.02 ± 0.01^{A} (4)	0.03 ± 0.02^{A}	0.03 ± 0.01^{A}	0.08 ± 0.10^{a}
Nitrate: Phosphate	15.7 ± 8.5^{A}	10.9 ± 6.4$^{A, B}$	5.3 ± 2.9^{B}	17.7 ± 17.2$^{A, B}$	81.5 ± 27.7^{A} (4)	42.5 ± 41.2^{A}	8.3 ± 8.7^{B}	37.0 ± 54.0$^{a, b}$
Silicate (μmol L^{-1})	1.35 ± 0.38^{A}	1.04 ± 0.50$^{A, B}$	0.69 ± 0.47^{B}	0.91 ± 0.50$^{A, B}$	1.53 ± 0.33^{A} (4)	1.29 ± 0.42^{A}	0.48 ± 0.17^{B}	1.03 ± 0.80$^{a, b}$
Chl*a* (μg L^{-1})	1.07 ± 0.36^{A}	0.32 ± 0.13^{B}	0.23 ± 0.11^{B}	0.57 ± 0.33^{A}	0.50 ± 0.20^{A}	0.27 ± 0.12$^{A, B}$	0.14 ± 0.03^{B} (5)	0.33 ± 0.19$^{a, b}$ (5)
POC (μmol L^{-1})	12.4 ± 4.5^{A}	11.0 ± 3.7^{A} (5)	11.8 ± 5.4^{A}	13.1 ± 9.4^{A}	8.8 ± 2.1^{A} (3)	10.8 ± 3.4^{A}	10.2 ± 4.8^{A}	9.7 ± 5.1^{a}
PON (μmol L^{-1})	1.7 ± 0.7^{A}	1.6 ± 0.6^{A} (5)	1.7 ± 1.0^{A}	2.0 ± 1.6^{A}	1.0 ± 0.3^{A} (3)	1.3 ± 0.6^{A}	1.1 ± 0.6^{A}	2.3 ± 3.0^{a}
PHA (×10^{5} cells mL^{-1})	9.04 ± 3.09^{A}	10.21 ± 4.04^{A}	8.35 ± 1.64^{A}	9.69 ± 2.51^{A}	0.17 ± 0.10^{A}	0.28 ± 0.10$^{A, B}$	0.30 ± 0.07$^{A, B}$ (5)	0.43 ± 0.17^{b} (5)
TEP (μg XG eq L^{-1})	32.2 ± 9.9^{A}	34.5 ± 22.0^{A}	42.3 ± 25.2^{A}	33.9 ± 24.5^{A}	25.8 ± 20.2^{A} (4)	29.2 ± 8.7^{A}	57.2 ± 38.3^{A}	28.2 ± 23.6^{a}
CSP (μg BSA eq L^{-1})	8.8 ± 3.8^{A} (5)	15.5 ± 6.7^{A}	11.0 ± 4.6^{A} (7)	12.1 ± 8.0^{A} (6)	11.0 ± 6.6$^{A, B}$ (4)	19.8 ± 2.5^{A}	12.8 ± 4.3$^{A, B}$ (4)	9.3 ± 4.6^{b} (5)
TEP: Chl*a* (μg XG eq μg $^{-1}$)	37.0 ± 26.3^{A}	126 ± 76.9$^{A, B}$	202 ± 123^{B}	60.2 ± 24.8^{B}	48.8 ± 39.9^{A} (4)	136 ± 98.2$^{A, B}$	444 ± 314^{B} (5)	94.7 ± 86.1^{b} (5)
CSP: Chl*a* (μg BSA eq μg $^{-1}$)	9.0 ± 3.8^{A} (5)	53.2 ± 23.5^{B}	59.0 ± 18.0^{B} (7)	23.2 ± 16.4^{A} (6)	20.5 ± 13.7^{A} (4)	87.8 ± 51.5^{B}	86.2 ± 25.8$^{A, B}$ (3)	42.9 ± 47.0$^{a, b}$ (4)
TEP: C (μg XG eq μg $^{-1}$)	1.09 ± 0.28^{A}	1.27 ± 0.83^{A}	2.26 ± 1.31^{A}	1.57 ± 0.93^{A}	1.60 ± 0.40^{A} (4)	2.69 ± 1.30^{B}	5.84 ± 3.55^{B} (5)	1.93 ± 1.44$^{a, b}$ (5)
CSP: C (μg BSA eq μg $^{-1}$)	0.39 ± 0.27^{A} (5)	0.53 ± 0.22^{A}	0.62 ± 0.24^{A} (7)	0.54 ± 0.28^{A} (6)	0.78 ± 0.28$^{A, B}$ (4)	1.86 ± 0.72^{A}	1.23 ± 0.41$^{A, B}$ (3)	0.70 ± 0.06^{b} (4)
TEP: POC (μg XG eq μg $^{-1}$)	0.2 ± 0.1^{A}	0.2 ± 0.1^{A} (5)	0.4 ± 0.3^{A}	2.8 ± 1.5^{A}	3.6 ±1.5$^{A, B}$ (3)	2.7 ±0.5^{B}	5.5 ± 2.2^{A}	3.1 ± 2.0^{b}
CSP: POC (μg BSA eq μg $^{-1}$)	0.8 ± 0.4^{A} (5)	1.6 ± 1.0^{A} (5)	1.0 ± 0.8^{A} (7)	1.1 ± 0.6^{A} (6)	1.4 ±0.4^{A} (3)	2.0 ±0.7^{A}	1.8 ±0.9^{A} (4)	1.1 ±0.5^{a} (5)

(continued)

Table 1. *(continued)*

	BBMO[b]				EOS[b]			
Variable[a]	Winter ($n = 6$)[c]	Spring ($n = 6$)	Summer ($n = 11$)	Fall ($n = 7$)	Winter ($n = 5$)	Spring ($n = 4$)	Summer ($n = 6$)	Fall ($n = 6$)
C: Chl*a* (μg μg $^{-1}$)	37.5 ± 26.8^{A}	99.6 ± 21.3^{B}	89.1 ± 16.2^{B}	43.3 ± 17.6^{A}	31.2 ± 20.1^{A}	47.4 ± 15.8$^{A, B}$	74.0 ± 24.3^{B} (5)	55.2 ± 52.0$^{a, b}$ (5)
POC: Chl*a* (μg μg $^{-1}$)	154 ± 73$^{A, C}$	452 ± 231$^{B, C}$(5)	712 ± 427^{B}	300 ± 184$^{A, C}$	204 ± 49^{A} (3)	565 ± 297$^{A, B}$	992 ± 413^{B} (5)	429 ± 253$^{a, b}$ (5)

BBMO = Blanes Bay Microbial Observatory; EOS = L'Estartit Oceanographic Station; XG = Xanthan Gum.

[a]MLD indicates mixed layer depth; Chl*a*, chlorophyll *a*; POC, particulate organic carbon; PON, particulate organic nitrogen; PHA, prokaryotic heterotrophic abundance; TEP, transparent exopolymer particles; CSP, Coomassie stainable particles; C, carbon in phytoplankton biomass; and daily solar radiation dose, average previous 24 h.

[b]Superscripted capital letters denote significantly different ($P < 0.05$) groups after nonparametric analysis of varaince followed by Mann Whitney tests.

[c]In parentheses is the sample number (n) whenever it differed from the one reported in the column heading.

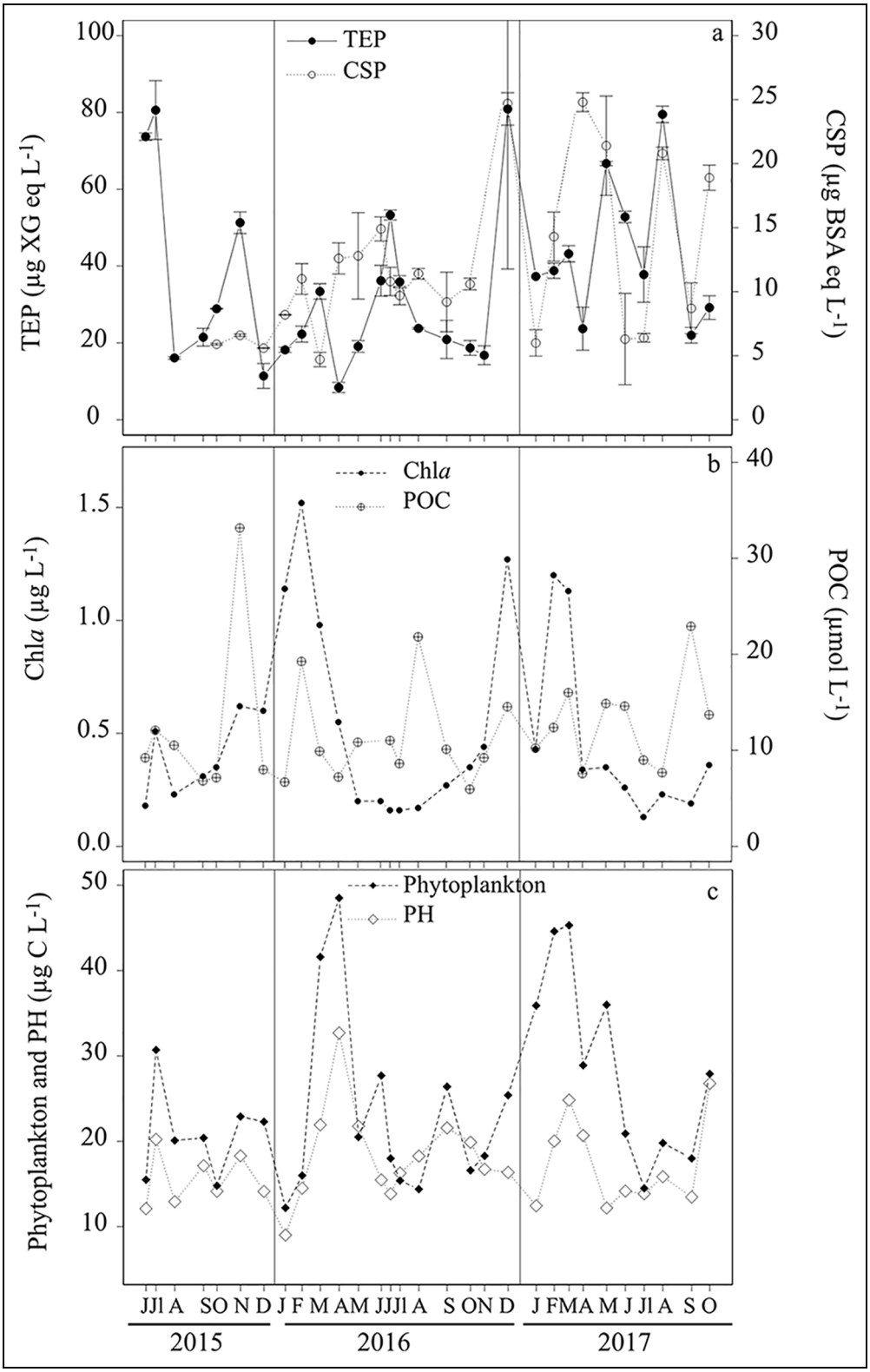

Figure 2. Surface values of chemical and biological variables in the Blanes Bay Microbial Observatory. Concentrations of (a) transparent exopolymer particles and Coomassie stainable particles, (b) particulate organic carbon and chlorophyll *a*, and (c) phytoplankton and prokaryotic heterotrophic biomasses. Each tick on the *x*-axis indicates the monthly sampling date starting in June 2015 (Jl indicates July). Error bars represent standard error of the mean ($n = 2$). DOI: https://doi.org/10.1525/elementa.2020.00165.f2

Dinoflagellates had maxima in late spring, but coccolithophores did not present clear seasonal variations at either of the stations (Figures S1 and S2).

Regarding the entire sampled water column at EOS, *Prochlorococcus* biomass presented high values at 50 m in the summers of 2015 and 2017. *Synechococcus* showed

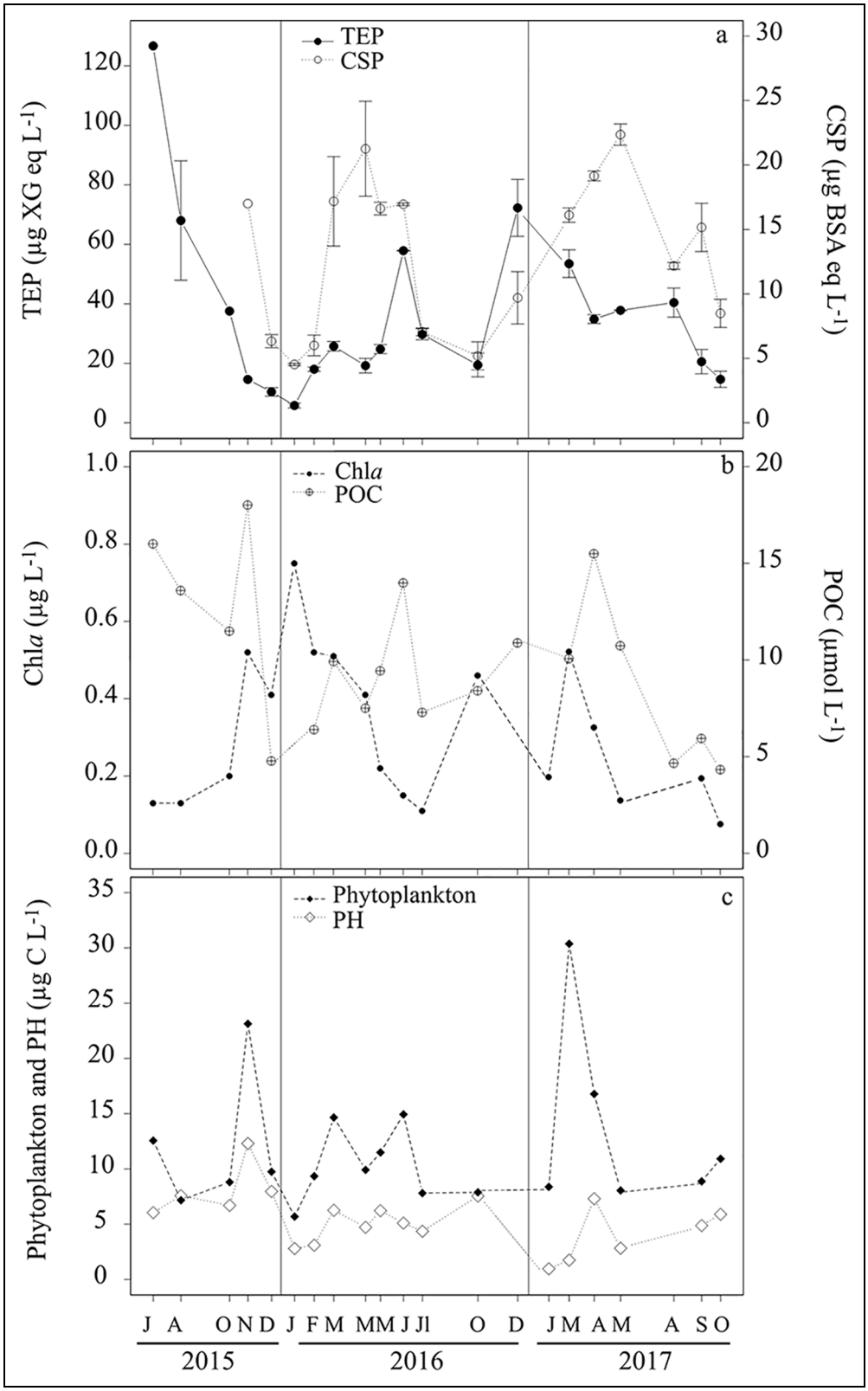

Figure 3. Surface values of chemical and biological variables in L'Estartit Oceanographic Station. Concentrations of (a) transparent exopolymer particles and Coomassie stainable particles, (b) particulate organic carbon and chlorophyll *a*, and (c) phytoplankton and prokaryotic heterotrophic biomasses. Each tick on the *x*-axis indicates the monthly sampling date starting in June 2015 (Jl indicates July). Error bars represent standard error of the mean ($n = 2$). DOI: https://doi.org/10.1525/elementa.2020.00165.f3

Table 2. Spearman correlations between transparent exopolymer particle (TEP) concentration and other environmental and biological variables in the sea surface at BBMO and EOS during the 2015–2017 period. DOI: https://doi.org/10.1525/elementa.2020.00165.t2

		BBMO[b]			EOS[b]		
Dependent Variable	Independent Variable[a]	*r*	*P*	*n*	*r*	*P*	*n*
TEP (μg XG eq L^{-1})	Temperature (°C)	ns[c]	ns	30	ns	ns	20
	Salinity	**−0.46**	**0.012**	**29**	**−0.48**	**0.039**	**19**
	Stratification index (°C)	ns	ns	29	ns	ns	20
	Water transparency (m)	ns	ns	30	ns	ns	20
	Daily solar radiation dose (Wm^{-2})	0.36	0.056	29	**0.58**	0.020	16
	Nitrate (μmol L^{-1})	ns	ns	30	ns	ns	20
	Phosphate (μmol L^{-1})	ns	ns	30	ns	ns	20
	Silicate (μmol L^{-1})	ns	ns	30	**−0.47**	0.036	20
	CSP (μg BSA eq L^{-1})	ns	ns	27	ns	ns	17
	Chl*a* (μg L^{-1})	ns	ns	30	**−0.47**	0.047	18
	Prochlorococcus (μg C L^{-1})	**−0.51**	0.004	30	**−0.61**	0.008	18
	Synechococcus (μg C L^{-1})	–0.36	0.051	30	ns	ns	18
	Picoeukaryotes (μg C L^{-1})	ns	ns	30	ns	ns	18
	Nanoeukaryotes (μg C L^{-1})	**0.40**	0.028	30	ns	ns	18
	Dinoflagellates (μg C L^{-1})	**0.50**	0.005	30	ns	ns	18
	Diatoms (μg C L^{-1})	**0.44**	0.015	30	ns	ns	18
	Coccolithophores (μg C L^{-1})	ns	ns	30	ns	ns	18
	Phytoplankton biomass (μg C L^{-1})	ns	ns	30	ns	ns	18
	POC (μmol L^{-1})	**0.41**	0.028	29	**0.50**	0.029	19
	PON (μmol L^{-1})	ns	ns	29	ns	ns	19
	PHA (x10^3 cells mL^{-1})	ns	ns	30	ns	ns	18

BBMO = Blanes Bay Microbial Observatory; EOS = L'Estartit Oceanographic Station; XG = Xanthan Gum.

[a]CSP indicates Coomassie stainable particles; Chl*a*, chlorophyll *a*; POC, particulate organic carbon; PON, particulate organic nitrogen; PHA, prokaryotic heterotrophic abundance.

[b]*r* is Spearman's correlation coefficient, where bold font indicates significance at $P < 0.05$; *P*, level of significance; *n*, sample size.

[c]not significant.

maximum concentrations at 20 m and/or 40 m in spring and summer. Diatom biomass was very high in the upper 50 m in November 2015 (Figure S3).

3.5. Variations of TEP and CSP in relation to Chl*a*, biomass, and POC

The average surface TEP: Chl*a* ratio was highest in summer at both stations, as was the ratio of TEP to phytoplankton carbon biomass (TEP: C; **Table 1**, **Figure 5**). The average surface CSP: Chl*a* ratio was higher in spring and summer, whereas the CSP: C ratio was higher in summer at BBMO and in spring at EOS (**Table 1**). The minimum values of TEP: Chl*a* and CSP: Chl*a* occurred in winter at both sites (**Table 1**). The ratio of carbon biomass to Chl*a* (C: Chl*a*) showed a clear seasonal cycle, with the lowest values in winter and fall (generally below 50) and the highest in spring and summer (generally above 50; **Figure 5**, **Table 1**). The POC: Chl*a* ratios were also higher in summer and lower in winter at both stations (**Table 1**). The TEP: POC ratios peaked in summer, while the CSP: POC ratios peaked in spring (**Table 1**).

The estimated contribution of TEP-C to the POC pool at BBMO and EOS (surface) ranged between 4% and 44% (average ± *SD* of 14% ± 9%) and between 3% and 37% (average of 16% ± 9%), respectively. TEP-C was within the ranges of phytoplankton and prokaryotic heterotroph biomass, and TEP-C contributed the most to the nondetrital particulate carbon pool in summer at EOS (**Figure 6**).

3.6. Environmental and biological variables as potential predictors of seasonal TEP and CSP dynamics

At BBMO, the variable that best correlated to TEP variability was dinoflagellate abundance ($r = 0.50$, $P = 0.005$,

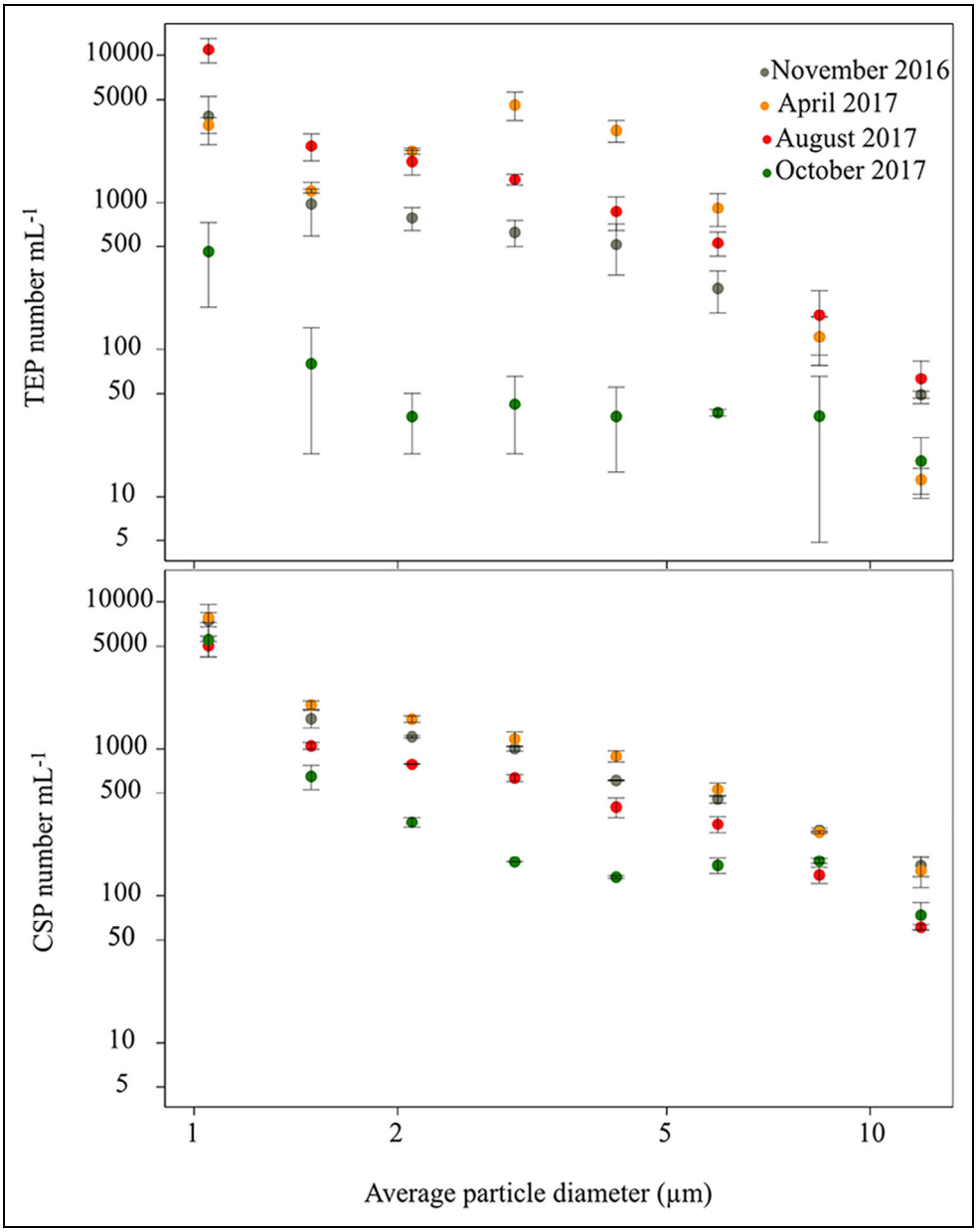

Figure 4. Size distributions of transparent exopolymer particles (TEP; top panel) and Coomassie stainable particles (CSP; bottom panel). Size distributions (number mL^{-1}) were obtained with the microscopic method for 4 samplings at the Blanes Bay Microbial Observatory, 1 in November of 2016 and the others in April, August, and October of 2017. Particle numbers are binned by their mean diameter: those ranging from 0 to 1.3 µm are grouped as 1.0 µm; 1.3 to 1.8 µm, as 1.5 µm; 1.8 to 2.5 µm, as 2.1 µm; 2.5 to 3.5 µm, as 3.0 µm; 3.5 to 5.0 µm, as 4.2 µm; 5.0 to 7.0 µm, as 6.0 µm; 7.0 to 10.0 µm, as 8.5 µm; and 10.0 to 14.0 µm, as 12.0 µm. In November 2016, the total area of TEP and CSP averaged 14 $\pm$ 12 and 38 $\pm$ 5 mm^2 L^{-1}, respectively. In April 2017, they averaged 41 $\pm$ 12 and 42 $\pm$ 10 mm^2 L^{-1}, respectively; in August 2017, 25 $\pm$ 7 and 19 $\pm$ 4 mm^2 L^{-1}, respectively; and in October 2017, 6 $\pm$ 3 and 16 $\pm$ 1 mm^2 L^{-1}, respectively. Error bars represent standard error of the mean (n = 2). Note log scale for axes. DOI: https://doi.org/10.1525/elementa.2020.00165.f4

n = 30), followed by diatoms and nanoeukaryotes (**Table 2**). However, there was no significant relationship between TEP and Chl*a* or total phytoplankton biomass. On the other hand, *Prochlorochoccus* showed a significant negative correlation with TEP (**Table 2**). CSP were not significantly correlated with any of the studied biological and environmental variables.

At EOS, TEP correlated positively only with the daily solar radiation dose (r = 0.58, P = 0.020, n = 16) and negatively with Chl*a* (r = –0.47, P = 0.047, n = 18), *Prochlorococcus* (r = –0.61, P = 0.008, n = 18), and silicate (r = –0.47, P = 0.036, n = 18). CSP, among all studied variables, was only correlated, positively, with total phytoplankton biomass (r = 0.53, P < 0.044, n = 15).

Unlike TEP concentrations, the ratios of TEP to Chl*a* and phytoplankton biomass correlated positively with solar radiation dose at both stations and negatively with nitrate, except for TEP: C at BBMO (**Table 3**). Similarly, CSP

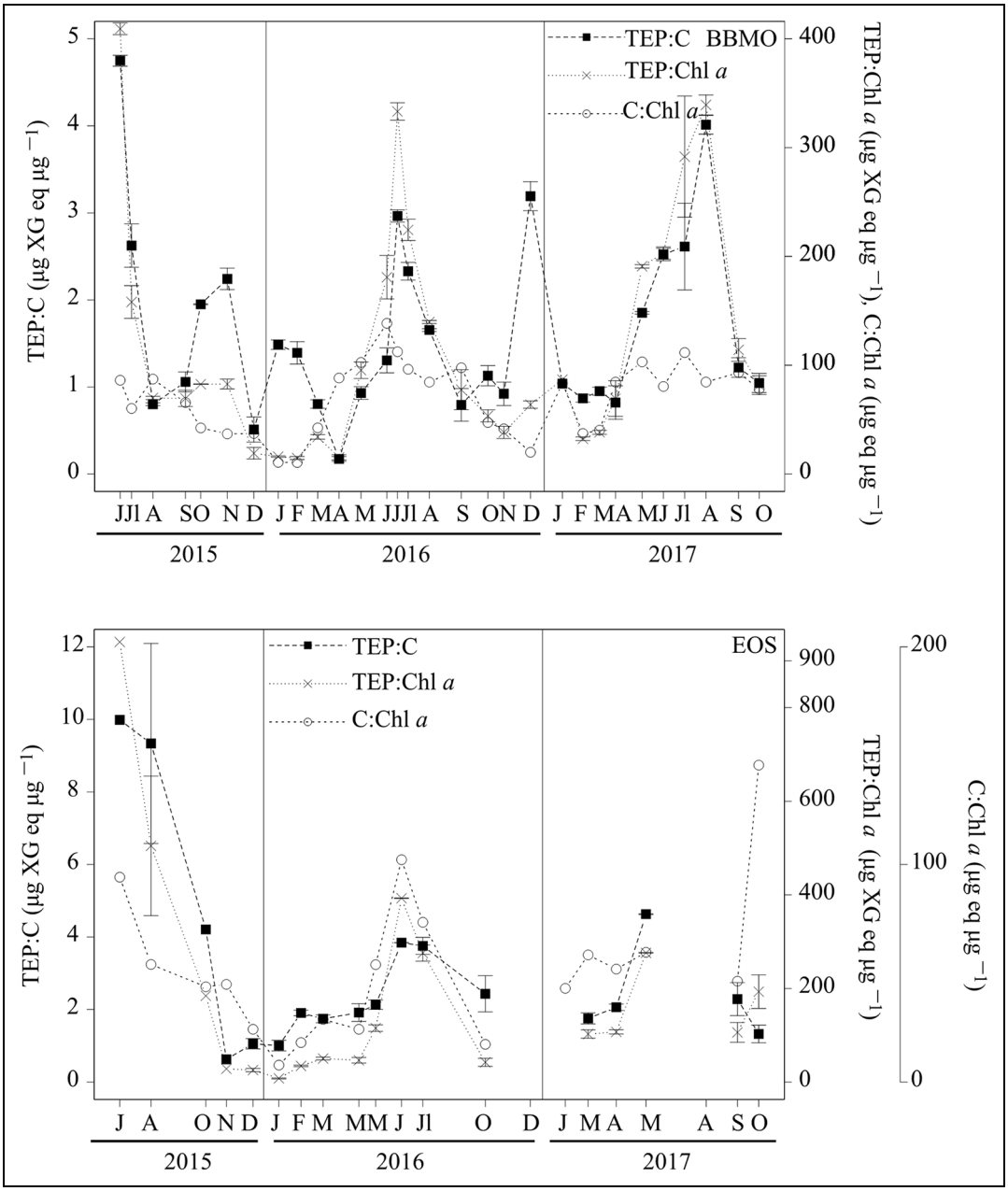

Figure 5. Ratios of TEP: C, TEP: Chla, and C: Chla over the BBMO (top) and EOS (bottom) time series. TEP indicates transparent exopolymer particles ($n = 2$); C, carbon in phytoplankton biomass ($n = 1$); Chla, chlorophyll a ($n = 2$); BBMO, Blanes Bay Microbial Observatory; and EOS, L'Estartit Oceanographic Station. Each tick on the *x*-axis indicates the monthly sampling date starting in June 2015 (Jl indicates July). Error bars represent standard error of the mean. DOI: https://doi.org/10.1525/elementa.2020.00165.f5

to Chl*a* ratios correlated positively with solar radiation dose ($r = 0.75$, $P < 0.001$, $n = 23$ at BBMO and $r = 0.83$, $P = 0.003$, $n = 13$ at EOS) and negatively with nitrate ($r = –0.62$, $P = 0.001$, $n = 23$ at BBMO and $r = –0.78$, $P < 0.001$, $n = 13$), but CSP to phytoplankton biomass ratios correlated only with nitrate at EOS ($r = –0.59$, $P = 0.024$, $n = 13$).

The vertical distribution of TEP coincided with that of dinoflagellate abundance, whereas CSP peaks coincided with relatively high *Synechococcus* abundance (Figure S3).

3.7. TEP and CSP distribution along the coast-to-open sea transect

Surface TEP concentrations ranged from 21.5 to 36.5 µg XG eq L^{-1} (average ± *SD* of 30.7 ± 5.4 µg XG eq L^{-1}) and increased from the coast to the open ocean (**Figure 7**). Surface CSP concentrations, which varied between 2.3 and 8.7 µg BSA eq L^{-1} (average of 5.2 ± 2.1 µg BSA eq L^{-1}), decreased from the coast to the slope and beyond (**Figure 7**), that is, opposite to TEP. Among the variables measured at surface, TEP concentrations were not correlated with any, whereas CSP correlated significantly and positively

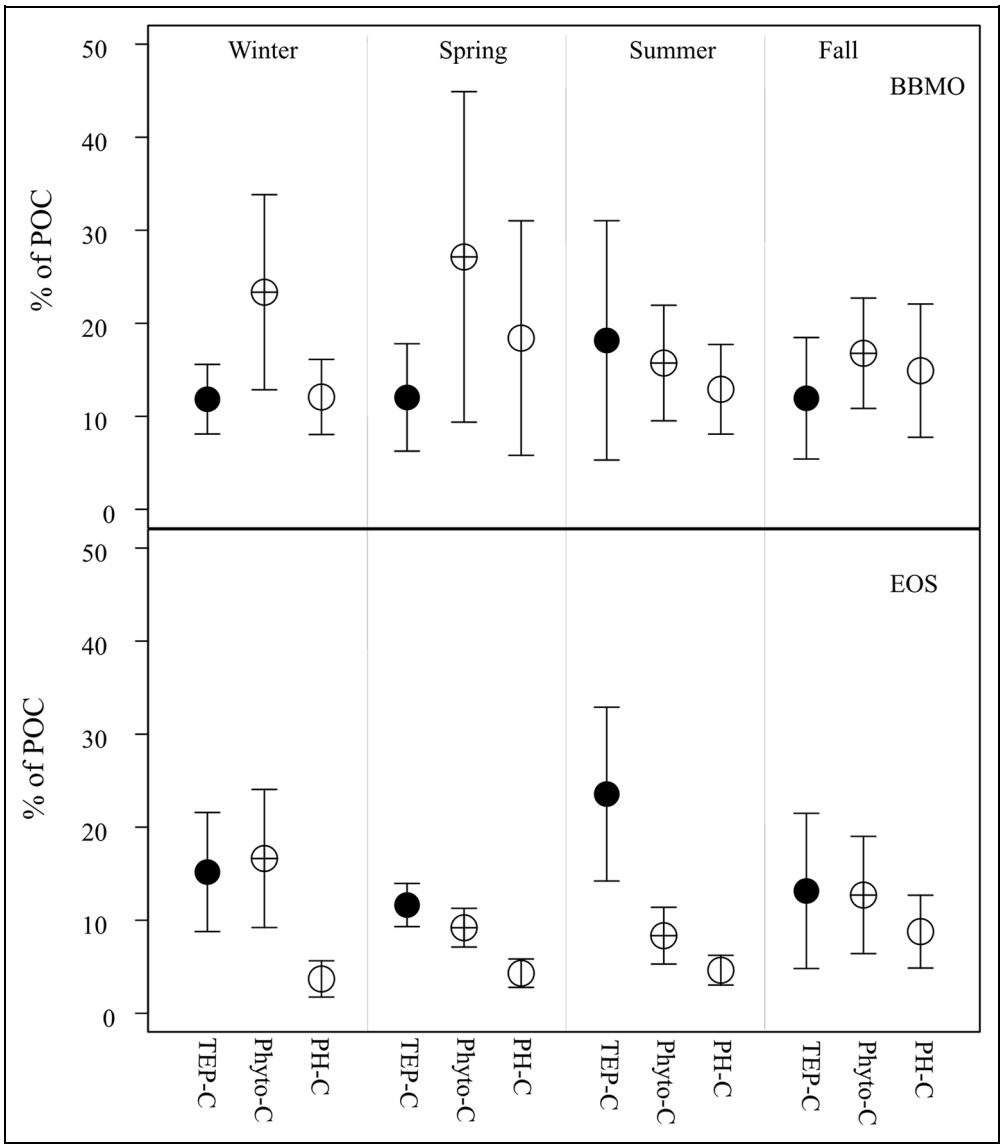

Figure 6. Contribution of transparent exopolymer particles (TEP) to particulate organic carbon (POC). Percentage carbon contribution of TEP (TEP-C), phytoplankton biomass (Phyto-C), and prokaryotic heterotroph biomass (PH-C) to the POC pool across seasons in surface waters of the Blanes Bay Microbial Observatory (BBMO, top panel) and L'Estartit Oceanographic Station (EOS, bottom panel). Symbols represent seasonal means; error bars represent standard deviations. From Winter to Fall samplings (left to right), *n* values were 6, 6, 11, and 7 at BBMO and 3, 4, 5–6, and 5–6 at EOS, where $n = 5$ for Phyto-C and PH-C and $n = 6$ for TEP-C at EOS. DOI: https://doi.org/10.1525/elementa.2020.00165.f6

with Chl*a* ($r = 0.93$, $P = 0.003$, $n = 7$) and nanoeukaryotes ($r = 0.86$, $P = 0.024$, $n = 7$).

TEP and CSP concentrations were generally lower at the depth of the DCM (average of 11.4 $\pm$ 3.6 µg XG eq L^{-1} for TEP and 2.9 $\pm$ 0.6 µg BSA eq L^{-1} for CSP) than at surface, despite higher Chl*a* levels in the DCM (**Figure 7**).

4. Discussion

We present the first simultaneous measurements of the distribution of TEP and CSP concentrations over 2 seasonal cycles in the Mediterranean Sea. The methods used to quantify these particles are based on the capability of different dyes to stain acidic polysaccharides and proteins, respectively (Passow and Alldredge, 1995; Cisternas-Novoa et al., 2014). However, the actual composition of the organic particles is unknown and depends on their sources and degradation processes (Passow, 2012). Particles probably consist of a mixture of TEP and CSP, along with other organic substances, inorganic molecules, and microbes. For instance, differential activities of extracellular enzymes or exoenzymes (e.g., protease or aminopeptidase vs. glucosidase activities) on marine aggregates (Smith et al., 1992; Piontek et al., 2009) could lead to changes in the relative proportion of TEP and CSP. In recent years, attempts have been made to elucidate whether these stained particle types (TEP and CSP) are in fact the same particles or not (Cisternas-Novoa et al., 2015; Thornton et al., 2016; Thornton and Chen, 2017), and the results have suggested that they mostly comprise different particulate substances. Our findings also support that TEP and CSP

Table 3. Spearman correlations between selected ratios (along with chlorophyll *a* concentration) and the daily solar radiation dose (Wm^{-2}) and nitrate concentration ($\mu mol\ L^{-1}$). DOI: https://doi.org/10.1525/elementa.2020.00165.t3

		BBMO[b]			EOS[b]		
Dependent Variable[a]	Independent Variable	*r*	*P*	*n*	*r*	*P*	*n*
TEP: Chl*a*	Daily solar radiation dose	**0.74**	<0.001	30	**0.96**	<0.001	18
TEP: C	Daily solar radiation dose	**0.41**	0.027	30	**0.78**	0.001	18
CSP: Chl*a*	Daily solar radiation dose	**0.75**	<0.001	23	**0.83**	0.003	13
CSP: C	Daily solar radiation dose	ns[c]	ns	24	ns	ns	13
Chl*a*	Daily solar radiation dose	**−0.72**	<0.001	30	**−0.80**	<0.001	18
C: Chl*a*	Daily solar radiation dose	**0.66**	<0.001	30	**0.87**	<0.001	18
TEP: Chl*a*	Nitrate	**−0.62**	<0.001	30	**−0.80**	<0.001	18
TEP: C	Nitrate	ns	ns	30	−0.63	0.005	18
CSP: Chl*a*	Nitrate	**−0.62**	0.001	24	**−0.78**	<0.001	15
CSP: C	Nitrate	ns	ns	24	−0.59	0.024	15

[a]TEP indicates transparent exopolymer particles; Chl*a*, chlorophyll *a*; C, carbon in phytoplankton biomass; and CSP, Coomassie stainable particles.

[b]*r* is Spearman's correlation coefficient, where bold font indicates significance at $P < 0.05$; *p*, level of significance; *n*, sample size.

[c]Not significant.

correspond to different types of particles, as they presented uncorrelated temporal dynamics over seasonal cycles at the 2 studied coastal sites (**Figures 2** and **3**, **Table 2**) and also different vertical distributions (Figure S3). These differences also suggest that they are likely produced by different organisms and/or subject to different aggregation and degradation processes, as suggested in previous studies (Cisternas-Novoa et al., 2015; Thornton et al., 2016; Thornton and Chen, 2017).

The absence of parallel temporal patterns of TEP and CSP, however, does not totally preclude that both particles are the same, at least in some cases. In fact, marine organic particles have heterogeneous chemical compositions, and both carbohydrate-rich and proteinaceous regions can coexist in the same aggregate (Busch et al., 2017). For instance, Dreshchinskii and Engel (2017) observed that TEP and CSP dynamics were coupled during 2 seasonal cycles in the Baltic Sea, both in the SML and in SSW, which contrasts with our results. However, visual examination of the particles with a FlowCAM (Cisternas-Novoa et al. 2015) or through microscopic examination (Thornton et al., 2016) led to the conclusion that Alcian Blue and CBB generally stain different particle types. In our case, we can conclude that, if both types of particles coexisted in the same aggregates, their TEP and the CSP contents in those aggregates varied independently: A large proportion of the pelagic aggregates we sampled contained Alcian-Blue stainable substances but no CBB stainable substances, as well as the reverse.

4.1. Dynamics of TEP and CSP over the seasonal cycle in the NW Mediterranean Sea

The peak of TEP found in December 2016 at both stations was likely related to freshwater discharges, as it coincided with a sharp decrease of salinity and an increase of nitrate at BBMO and phosphate at EOS. The BBMO is known to receive inputs of nutrients and terrestrial carbon sporadically during storm periods (Guadayol et al., 2009b). Aside from this exceptional sampling time, the maximum TEP concentrations found in early summer at both stations (**Figures 2**, **3**, and S4) are in accordance with previous studies in the Mediterranean Sea (Beauvais et al., 2003; Ortega-Retuerta et al., 2018). Ortega-Retuerta et al. (2018) suggested that TEP maxima in summer could be due to the increase of TEP production under nutrient limitation, the presence of specific phytoplankton groups, and/or the accumulation of TEP due to positive buoyancy during water stratification. This study expands the previous temporal study conducted at the BBMO (Ortega-Retuerta et al., 2018) by incorporating information about phytoplankton biomass and solar radiation dose, which appear to be relevant factors.

The range of our TEP concentrations across the 2 stations (5.8–127 $\mu g\ XG\ eq\ L^{-1}$) was similar to that found by Ortega-Retuerta et al. (2018) at the BBMO during the 3 previous years (11.3–289 $\mu g\ XG\ eq\ L^{-1}$) and by Iuculano et al. (2017a) in a rocky shore site of the Balearic Sea (4.6–90.6 $\mu g\ XG\ eq\ L^{-1}$), while it was generally lower than the range found in a coastal site accumulating *Posidonia oceanica* leaf litter in the Balearic Sea (26.8–1,880 $\mu g\ XG\ eq\ L^{-1}$; Iuculano et al., 2017a).

CSP concentrations at both stations (4.5–24.8 $\mu g\ BSA\ eq\ L^{-1}$) were within the range of the few previous published studies (**Table 4**). The highest CSP concentrations were found in spring; however, according to the harmonic analysis, the seasonal pattern was only significant at EOS (**Figures 2**, **3**, and S4). Cisternas-Novoa et al. (2015) found steady CSP concentrations throughout the

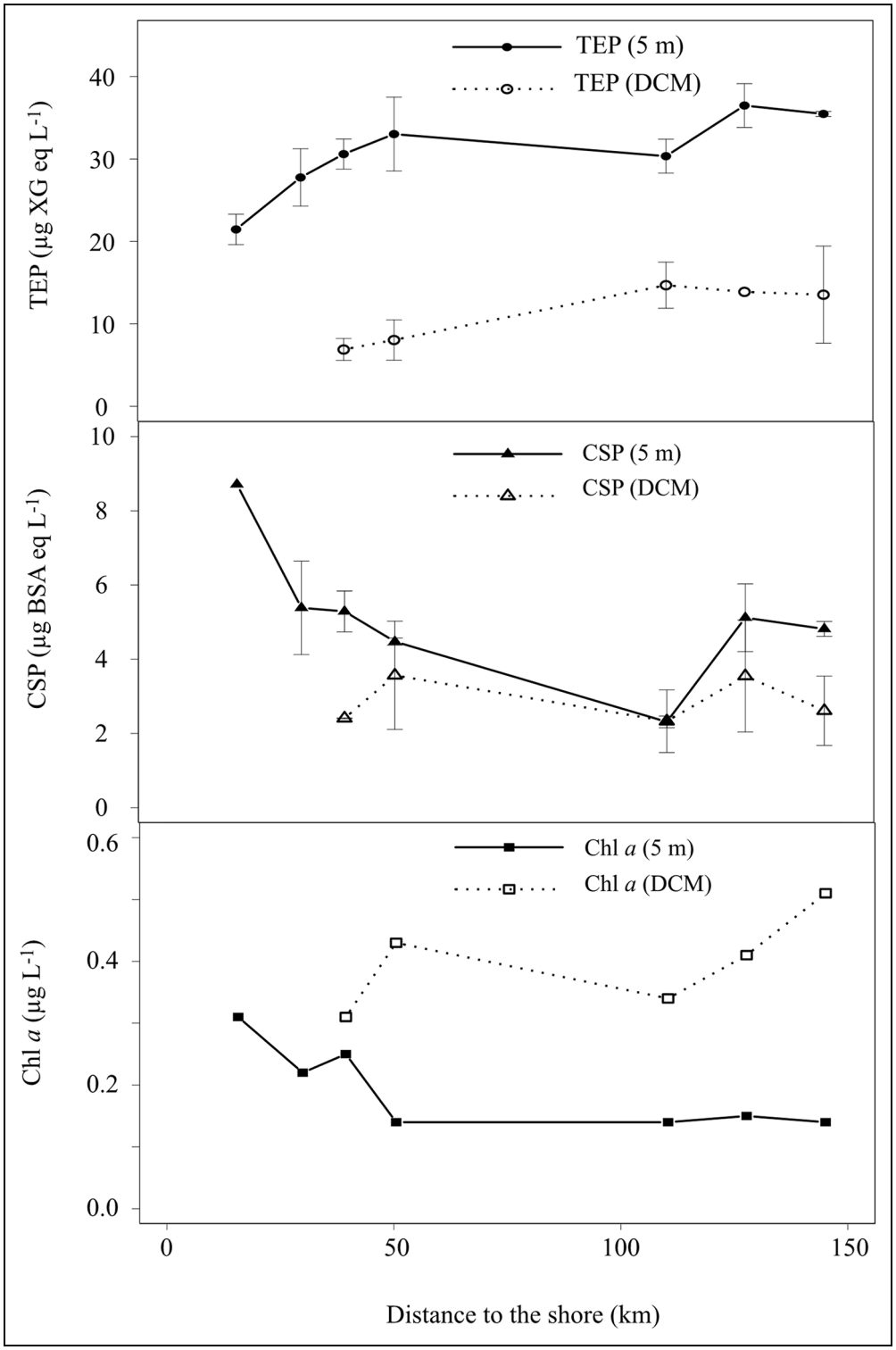

Figure 7. Concentrations of transparent exopolymer particles (TEP) and Coomassie stainable particles (CSP) along a coastal–offshore transect. Concentrations of TEP (circles), CSP (triangles), and chlorophyll a (squares) at 5 m (closed symbols) and the deep chlorophyll maximum (DCM, open symbols) as a function of distance to the shore. Note that DCM was only present at the deeper (farther offshore) stations. Error bars represent standard error of the mean ($n = 2$). DOI: https://doi.org/10.1525/elementa.2020.00165.f7

year in the upper 100 m of the Sargasso Sea, while Dreschchinskii and Engel (2017) observed the highest CSP abundance during the winter and summer periods in the Baltic Sea, with frequent oscillations in the total area of CSP.

4.2. Main drivers of TEP and CSP dynamics

We first examined Chl*a*, typically used as an indicator of phytoplankton biomass, as a potential driver of TEP and CSP dynamics, but Chla did not correlate positively with TEP or CSP at either of our sampling sites, and correlated

Table 4. Compilation of published Coomassie stainable particle (CSP) concentrations (mean ± *SD*, range), chlorophyll *a* (Chl*a*) concentrations (mean ± *SE*, range; μg L^{-1}), and CSP: Chl*a* ratios (mean ± *SE* ranges) and CSP: Chl*a* ratios (mean ± *SE*, ranges). DOI: https://doi.org/10.1525/elementa.2020.00165.t4

Location	Time Frame	Depth (m)	CSP (μg BSA eq L^{-1})	Chl*a* (μg L^{-1})	CSP: Chl*a*	Reference
Sargasso Sea	February, May, August, and November 2012; May 2013	0–100	3.2 ± 0.7 to 22.4 ± 0.4	0.25–0.75[a]	—[b]	Cisternas-Novoa et al. (2015)
Baltic Sea	June 3–19, 2015	1 and 10	15–56 [a]	1.2 to 1.7	—	Cisternas-Novoa et al. (2019)
Northwestern Mediterranean Sea (BBMO and EOS)	October 2015–October 2017 (time-series study)	Surface	12.4 ± 6.0, 4.5–24.8	0.4 ± 0.3, 0.13–1.52	45.6 ± 35.7, 4.8–163	This study

[a]Extracted from graphs.

[b]No reported values.

negatively with TEP at EOS. Ortega-Retuerta et al. (2018) also found a negative correlation of TEP with Chl*a* (at BBMO). Some time-series studies have reported covariation between TEP and Chl*a* (Beauvais et al., 2003; Scoullos et al., 2006; Engel et al., 2017; Parinos et al., 2017), while this covariation was not found by others (Bhaskar and Bhosle, 2006; Taylor et al., 2014) or was only observed during certain periods of the year (Dreshchinskii and Engel, 2017). In our study, the C: Chl*a* ratio of phytoplankton changed throughout the year at both BBMO and EOS, in accordance with Gasol et al. (2016) and Gutiérrez-Rodríguez et al. (2010) for BBMO. Earlier work has shown that the ratio was usually higher in spring and summer driven by the high irradiance and low nutrients in these seasons (Geider et al., 1998). Consequently, Chl*a* cannot be considered a good indicator of phytoplankton biomass across seasons, and instead we used biomass estimates based on cell abundances, size or species-specific biovolumes, and volume-to-carbon conversion factors.

The findings that CSP correlated positively with total phytoplankton biomass at EOS, while TEP did not show this correlation at either of our sampling sites, support our initial hypothesis that CSP temporal variations, at least at the sea surface, are more closely related to phytoplankton biomass than those of TEP. Although primary production data are not available for our study years, the highest CSP concentrations of the time series (from late winter to early summer) coincide with the period of maximum primary production recorded in a 12-year study (2003–2014) at BBMO (Gasol et al., 2016). Gasol et al. (2016) also reported that Chl*a*-specific primary production (C production per unit of Chl*a*), measured with the ^{14}C method, was highest in summer and lowest in winter, likely due to higher photosynthetic efficiency of summer phytoplankton. Based on our observations, the higher Chl*a*-specific primary production in summer could be partially explained by enhanced production of TEP and CSP, as a portion of these particles would be retained on the filters used for the ^{14}C-PP measurements and thus taken as phytoplankton biomass produced de novo. Along these same lines, Alonso-Sáez et al. (2008) found that DOC release accounted for up to 45% of total primary production at BBMO, with a lower proportion in winter. Because DOC can self-assemble to form TEP, this release of primary production as DOC could have further contributed to higher TEP concentrations in spring and summer.

While CSP did not correlate with measured variables other than phytoplankton biomass (except for POC and PON at EOS), TEP correlated positively with the daily solar radiation dose at EOS (**Table 2**), and TEP: C correlated positively with the solar radiation dose at both stations, and negatively with nitrate at EOS (**Table 2**). These correlations could be indicative of either the stimulation of microbial TEP release by light stress, as suggested by Iuculano et al. (2017b), Agustí and Llabrés (2007), and Zamanillo et al. (2019a), or the enhancement of abiotic self-assembly of dissolved exopolymers into TEP (Shammi et al., 2017). The negative relationship of TEP: C with nitrate (**Table 2**) could be due to the stimulation of phytoplankton TEP production under nutrient limitation in summer, as suggested by Ortega-Retuerta et al. (2018). CSP: C was also negatively related with nitrate at EOS, but more research is needed to determine whether nutrient limitation stimulates CSP production.

Gasol et al. (2016) found relatively high saturating irradiances (high values for the light saturation parameter) all year round at BBMO, which is a phytoplankton feature typical of regions receiving relatively high light intensities. In winter, the observed light saturation values were close to the surface irradiance at the time of sampling, whereas in summer, they were close to the irradiance values observed at 5-m depth. This depth differential indicates that in summer, phytoplankton cells living above 5 m receive irradiances in excess of their saturating values, which may favor the production of TEP (Agustí and Llabrés, 2007).

Prokaryotic heterotrophs can influence TEP and CSP dynamics in the ocean not only through particle colonization and enzymatic degradation (Passow and Alldredge, 1994; Long and Azam, 1996) but also by producing TEP

(Radic et al., 2006; Ortega-Retuerta et al., 2019) or enhancing TEP and CSP production by phytoplankton (Gärdes et al., 2011). We showed previously that TEP dynamics at BBMO are correlated to exoenzyme activities (esterase, alkaline phosphatase, and beta-glucosidase; Ortega-Retuerta et al., 2018), but not to prokaryotic heterotrophic abundance. Our findings are consistent with their study, in that neither TEP nor CSP correlated with prokaryotic heterotrophic abundance, and phytoplankton abundance was a stronger predictor of the temporal variation of these 2 particle types.

Significant correlations between TEP or CSP dynamics and those of specific phytoplankton groups provide hints about the main producers of these particles at our study sites: TEP mainly correlated with dinoflagellates, diatoms, and nanoeukaryotes over time at the BBMO (**Table 2**), whereas CSP did not correlate with any group over time at either station, although at the vertical scale, CSP was best related to *Synechococcus*, as previously observed by Cisternas-Novoa et al. (2015).

4.3. Contribution of TEP, phytoplankton, and prokaryotic heterotrophs to POC

TEP contributed remarkably to the POC pool (overall range of 3%–44%), in similar proportions to those measured in the northeastern Atlantic Ocean (1.5%–68%; Harlay et al., 2009, 2010), but lower than many of the percentages reported across the Atlantic Ocean (28%–110% by Zamanillo et al., 2019b), the Mediterranean Sea (60% to >100% by Bar-Zeev et al., 2011; 14% to >100% by Parinos et al., 2017; 4% to >100% by Ortega-Retuerta et al., 2019) and the western Arctic Ocean (135%–179% by Yamada et al., 2015). This disparity across studies, where unrealistic TEP contributions higher than 100% abound, points to the uncertainty in the TEP-to-C conversion factor across systems and seasons. In alignment with Bar-Zeev et al. (2011), Parinos et al. (2017), and Zamanillo et al. (2019b), we used a conservative value (0.51 μg TEP-C μg XG eq^{-1}) from a range of conversion factors determined experimentally with cultured and natural marine diatoms (Engel and Passow, 2001). Other authors (Harlay et al., 2010; Yamada et al., 2015; Ortega-Retuerta et al., 2019) used higher values from the same seminal study (0.63–0.75 μg TEP-C μg XG eq^{-1}). In any case, the C content of TEP is expected to vary with their monomeric composition, which in turn depends on TEP origin (Engel and Passow, 2001); with this information lacking, comparisons of TEP carbon between oceanic studies is problematic. Another reason for the frequent oversizing of the TEP contribution to POC is merely methodological: TEP are measured on 0.4-μm pore-size filters because they are not retained quantitatively on the GF/F filters used for POC (Passow and Alldredge, 1995; Engel and Passow, 2001) and, therefore, an unknown fraction of TEP may be lost in the measured POC pool.

Despite these uncertainties and the use of a conservative conversion factor, in summer the estimated carbon in the form of TEP was higher than that of phytoplankton and prokaryotic heterotrophs, at least at EOS (**Figure 6**). TEP: POC also tended to be higher in summer in this site (**Table 1**), suggesting a higher TEP contribution to the POC pool in this season. A higher contribution might affect particle density: Particles with relatively higher TEP would be of lower density (Engel and Schartau, 1999) and, consequently, would present a lower sinking velocity or could even ascend (Azetsu-Scott and Passow, 2004; Mari et al., 2007) and accumulate at or near the surface. We hypothesize that the lower density of TEP-rich particles in summer would have also contributed to their observed accumulation in the sea surface (i.e., above 20 m at EOS), in conjunction with higher production rates under high light and nutrient limitation.

4.4. TEP and CSP size distribution

The microscopic examination provided evidence that, even though TEP were generally dominated by small particles as in previous studies (Passow and Alldredge, 1994; Mari and Burd, 1998; Harlay et al., 2009), their size distribution changed over time (**Figure 4**). The modal distribution of the April sample could be indicative of freshly produced TEP from a particular source, maybe a specific phytoplankton population, or to aggregation processes. The steeper TEP size distribution slope in August with respect to October could be related to solar radiation, which could either inhibit TEP aggregation into larger sizes or break up larger aggregates into small TEP, or both. By contrast, CSP size distributions were similar throughout the year, which we suggest hints at a lower aggregation potential of CSP compared to TEP.

4.5. Distribution of TEP and CSP in the coast-to-offshore transect

The different distribution patterns of TEP and CSP along the coast-to-offshore transect (**Figure 7**) indicate that the 2 particle types are also uncoupled on the spatial scale. Like the observations over the temporal scale, the positive correlation of CSP with Chl*a* illustrates that CSP variations are more directly linked to those of phytoplankton than TEP variations. Supporting that hypothesis, Arin et al. (1999) found higher concentrations of particulate protein and higher percentages of detrital protein in surface waters of the shore-most station than in the open sea along a coast-to-offshore transect in the NW Mediterranean Sea.

5. Conclusions

According to our results, TEP and CSP are most likely independent particle types as they presented uncoupled temporal dynamics at 2 coastal sites and uncoupled spatial distributions along a coast-to-offshore transect in the NW Mediterranean Sea. Taxonomy-segregated phytoplankton biomass was the main driver of both TEP and CSP concentrations: diatoms, dinoflagellates, and nanoeukaryotes each explained 40%–50% of TEP distribution at surface, with dinoflagellates covarying best with TEP over depth and *Synechococcus* abundances best matching CSP vertical profiles. While CSP are best explained by phytoplankton biomass, nutrient limitation and the release of phytoplankton carbon under saturating irradiance are suggested as additional drivers of the distribution and

temporal dynamics of TEP. The finding that 2 geographically close coastal sites exhibit similar temporal patterns of TEP concentration suggests that TEP variability indeed reflects a response to the environmental seasonality characteristic of this temperate oligotrophic region.

Data accessibility statement

The data are deposited at https://doi.org/10.5281/zenodo.5633941.

Supplemental files

The supplemental files for this article can be found as follows:

Figures S1–S4. PDF

Acknowledgments

We would like to thank all the Blanes Bay Microbial Observatory and L'Estartit Oceanographic Station team, especially Clara Cardelús, Vanessa Balagué, Àngel López-Sanz, Irene Forn, Raquel Gutiérrez, Carolina Antequera, Mara Abad, and Anselm Albiol, for their organization, sampling efforts, and ancillary measurements. We also want to thank Maria Castellví and Idaira Santos for helping with transparent exopolymer and Coomassie stainable particle measurements, and Jon Roa, Alexandra Loginova, Sonja Endres, Judith Piontek, Katja Lass, Ruth Flerus, Tania Klüver, Marie Massmig, and Birthe Zäncker for their technical support. We thank the scientists and technicians on board the RV *García del Cid* during the MIFASOL II cruise for providing environmental and logistic support. We also thank two anonymous reviewers for their constructive comments.

Funding

This research was funded by the Spanish Ministry of Economy and Competitiveness through projects PEGASO (CTM2012–37615), BIOGAPS (CTM2016–81008–R), REMEI (CTM2015-70340-R), and DOREMI (CTM12-34294) and the Generalitat de Catalunya, through funding to the Research Group on Marine Biogeochemistry and Global Change (2017 SGR1011) and that of Microbial Diversity and Function in Aquatic Systems (2017SGR/1568) and with the institutional support of the Severo Ochoa Center of Excellence accreditation (CEX2019-000928-S). MZ was supported by a FPU predoctoral fellowship (FPU13/04630) from the Spanish Ministry of Education and Culture. The EOS Monitoring Program is supported by the Institut de Ciències del Mar (ICM-CSIC) and the Parc Natural del Montgrí, les Illes Medes i el Baix Ter (Generalitat de Catalunya).

Competing interests

The authors declare that they have no conflict of interest.

Author contributions

Analyzed samples in the context of the Blanes Bay Microbial Observatory and L'Estartit Oceanographic Station time series, with the help of EOR and CCN: MZ.

Designed the study and analyzed data: EOR, RS, MZ.

Provided accompanying physical, chemical, and biological data: CM, JMG, JP, CP.

Helped with data contextualization: AE, CCN.

Wrote this article with the help of all coauthors: MZ, EOR, RS.

Approved the submission: All authors.

References

Agustí, S, Llabrés, M. 2007. Solar radiation-induced mortality of marine Pico-phytoplankton in the oligotrophic ocean. *Photochemistry and Photobiology* **83**: 793–801.

Alldredge, AL, Passow, U, Logan, BE. 1993. The abundance and significance of a class of large, transparent organic particles in the ocean. *Deep Sea Research Part I: Oceanographic Research Papers* **40**: 1131–1140.

Aller, JY, Kuznetsova, MR, Jahns, CJ, Kemp, PF. 2005. The sea surface microlayer as a source of viral and bacterial enrichment in marine aerosols. *Journal of Aerosol Science* **36**: 801–812.

Aller, JY, Radway, JC, Kilthau, WP, Bothe, DW, Wilson, TW, Vaillancourt, RD, Quinn, PK, Coffman, DJ, Murray, BJ, Knopf, DA. 2017. Size-resolved characterization of the polysaccharidic and proteinaceous components of sea spray aerosol. *Atmospheric Environment* **154**: 331–347.

Alonso-Sáez, L, Vázquez-Domínguez, E, Cardelús, C, Pinhassi, J, Sala, MM, Lekunberri, I, Balagué, V, Vila-Costa, M, Unrein, F, Massana, R, Simó, R, Gasol, JM. 2008. Factors controlling the year-round variability in carbon flux through bacteria in a coastal marine system. *Ecosystems* **11**: 397–409.

Aparicio, FL, Nieto-Cid, M, Calvo, E, Pelejero, C, Lopez-Sanz, A, Pascual, J, Salat, J, Sanchez-Perez, ED, La Fuente, P, Gasol, JM, Marrase, C. 2017. Wind-induced changes in the dynamics of fluorescent organic matter in the coastal NW Mediterranean. *Science of the Total Environment* **609**: 1001–1012.

Arin, L, Berdalet, E, Marrasé, C, Estrada, M, Guixa-Boixereu, N, Dolan, J. 1999. Particulate DNA and protein relative to microorganism biomass and detritus in the Catalano-Balearic Sea (NW Mediterranean) during stratification. *Journal of Plankton Research* **21**: 1299–1316.

Azam, F, Malfatti, F. 2007. Microbial structuring of marine ecosystems. *Nature Reviews Microbiology* **5**: 782–791.

Azetsu-Scott, K, Passow, U. 2004. Ascending marine particles: Significance of transparent exopolymer particles (TEP) in the upper ocean. *Limnology and Oceanography* **49**: 741–748.

Bar-Zeev, E, Berman, T, Rahav, E, Dishon, G, Herut, B, Berman-Frank, I. 2011. Transparent exopolymer particle (TEP) dynamics in the eastern Mediterranean Sea. *Marine Ecology Progress Series* **431**: 107–118.

Bar-Zeev, E, Passow, U, Castrillon, SR, Elimelech, M. 2015. Transparent exopolymer particles: From aquatic environments and engineered systems to

membrane biofouling. *Environmental Science & Technology* **49**: 691–707.

Beauvais, S, Pedrotti, ML, Villa, E, Lemée, R. 2003. Transparent exopolymer particle (TEP) dynamics in relation to trophic and hydrological conditions in the NW Mediterranean Sea. *Marine Ecology Progress Series* **262**: 97–109.

Behrenfeld, M. 2010. Abandoning Sverdrup's Critical Depth Hypothesis on phytoplankton blooms. *Ecology* **91**: 977–989.

Bhaskar, PV, Bhosle, NB. 2006. Dynamics of transparent exopolymeric particles (TEP) and particle-associated carbohydrates in the Dona Paula bay, west coast of India. *Journal of Earth System Science* **115**: 403–413.

Brooks, SD, Thornton, DCO. 2018. Marine aerosols and clouds. *Annual Review of Marine Science* **10**: 289–313.

Burd, AB, Jackson, GA. 2009. Particle aggregation. *Annual Review of Marine Science* **1**: 65–90.

Busch, K, Endres, S, Iversen, MH, Michels, J, Nöthig, E-M, Engel, A. 2017. Bacterial colonization and vertical distribution of marine gel particles (TEP and CSP) in the Arctic Fram Strait. *Frontiers in Marine Science* **4**: 166.

Calleja, ML, Duarte, CM, Prairie, YT, Agustí, S, Herndl, GJ. 2009. Evidence for surface organic matter modulation of air–sea CO_2 gas exchange. *Biogeosciences* **6**: 1105–1114.

Calvo-Díaz, A, Morán, XAG. 2006. Seasonal dynamics of picoplankton in shelf waters of the southern Bay of Biscay. *Aquatic Microbial Ecology* **42**: 159–174.

Cisternas-Novoa, C, Lee, C, Engel, A. 2014. A semi-quantitative spectrophotometric, dye-binding assay for determination of Coomassie Blue stainable particles. *Limnology and Oceanography: Methods* **12**: 604–616.

Cisternas-Novoa, C, Lee, C, Engel, A. 2015. Transparent exopolymer particles (TEP) and Coomassie stainable particles (CSP): Differences between their origin and vertical distributions in the ocean. *Marine Chemistry* **175**: 56–71.

Cisternas-Novoa, C, Le Moigne, FAC, Engel, A. 2019. Composition and vertical flux of particulate organic matter to the oxygen minimum zone of the central Baltic Sea: Impact of a sporadic North Sea inflow. *Biogeosciences* **16**: 927–947.

Claquin, P, Probert, I, Lefebvre, S, Veron, B. 2008. Effects of temperature on photosynthetic parameters and TEP production in eight species of marine microalgae. *Aquatic Microbial Ecology* **51**: 1–11.

Decho, AW. 1990. Microbial exopolymer secretions in ocean environments: Their role (s) in food webs and marine processes. *Oceanography and Marine Biology Annual Reviews* **28**: 73–153.

Dreshchinskii, A, Engel, A. 2017. Seasonal variations of the sea surface microlayer at the Boknis Eck times series station (Baltic Sea). *Journal of Plankton Research* **39**: 943–961.

Duarte, CM, Agustí, S, Vaqué, D. 2004. Controls on planktonic metabolism in the Bay of Blanes, northwestern Mediterranean littoral. *Limnology and Oceanography* **49**(6): 2162–2170.

Endres, S, Unger, J, Wannicke, N, Nausch, M, Voss, M, Engel, A. 2013. Response of Nodularia spumigena to pCO_2—Part 2: Exudation and extracellular enzyme activities. *Biogeosciences* **10**: 567–582.

Engel, A. 2009. Determination of marine gel particles, in Wurl, O ed., *Practical guidelines for the analysis of seawater*. Boca Raton, FL: CRC Press, Taylor & Francis Group: 125–142.

Engel, A, Borchard, C, Loginova, A, Meyer, J, Hauss, H, Kiko, R. 2015. Effects of varied nitrate and phosphate supply on polysaccharidic and proteinaceous gel particle production during tropical phytoplankton bloom experiments. *Biogeosciences* **12**: 5647–5665.

Engel, A, Delille, B, Jacqet, S, Riebesell, U, Rochelle-Newall, E, Terbrügen, A, Zondervan, I. 2004. Transparent exopolymer particles and dissolved organic carbon production by *Emiliania huxleyi* exposed to different CO_2 concentrations: A mesocosm experiment. *Aquatic Microbial Ecology* **34**: 93–104.

Engel, A, Endres, S, Galgani, L, Schartau, M. 2020. Marvelous marine microgels: On the distribution and impact of gel-like particles in the oceanic water-column. *Frontiers in Marine Science* **7**: 1–15.

Engel, A, Galgani, L. 2016. The organic sea-surface microlayer in the upwelling region off the coast of Peru and potential implications for air–sea exchange processes. *Biogeosciences* **13**: 989–1007.

Engel, A, Passow, U. 2001. Carbon and nitrogen content of transparent exopolymer particles (TEP) in relation to their Alcian Blue adsorption. *Marine Ecology Progress Series* **219**: 1–10.

Engel, A, Piontek, J, Metfies, K, Endres, S, Sprong, P, Peeken, I, Gabler-Schwarz, S, Nothig, EM. 2017. Inter-annual variability of transparent exopolymer particles in the Arctic Ocean reveals high sensitivity to ecosystem changes. *Scientific Reports* **7**:.4129.

Engel, A, Schartau, M. 1999. Influence of transparent exopolymer particles (TEP) on sinking velocity of Nitzschia closterium aggregates. *Marine Ecology Progress Series* **182**: 69–76.

Gärdes, A, Iversen, MH, Grossart, HP, Passow, U, Ullrich, MS. 2011. Diatom-associated bacteria are required for aggregation of *Thalassiosira weissflogii*. *ISME Journal* **5**: 436–445.

Gasol, JM, Cardelús, C, Morán, XAG, Balagué, V, Forn, I, Marrasé, C, Massana, R, Pedrós-Alió, C, Montserrat Sala, M, Simó, R, Vaqué, D, Estrada, M. 2016. Seasonal patterns in phytoplankton photosynthetic parameters and primary production at a coastal NW Mediterranean site. *Scientia Marina* **80**: 63–77.

Gasol, JM, Massana, R, Simó, R, Marrasé, C, Acinas, SG, Pedrós-Alió, C, Pelejero, C, Sala, MM, Calvo, E, Vaqué, D, Peters, F. 2012. Blanes Bay, in O'Brien, TD, Li, WKW, Morán, XAG eds., ICES phytoplankton

and microbial ecology status report 2010/2012. ICES Cooperative Research Report No. 313. 196 pp.

Gasol, JM, Morán, XAG. 2015. Flow cytometric determination of microbial abundances and its use to obtain indices of community structure and relative activity, in McGenity, TJ, Timmis, KN, Nogales, B eds., *Hydrocarbon and lipid microbiology protocols*. Berlin, Germany: Springer (Springer Protocols Handbooks). DOI: https://doi.org/10.1007/8623_2015_139.

Geider, RJ, Macintyre, HL, Kana, TM. 1998. A dynamic regulatory model of phytoplanktonic acclimation to light, nutrients, and temperature. *Limnology and Oceanography* **43**: 679–694.

Grossart, HP, Berman, T, Simon, M, Pohlmann, K. 1998. Occurrence and microbial dynamics of macroscopic organic aggregates (lake snow) in Lake Kinneret, Israel, in fall. *Aquatic Microbial Ecology* **14**: 59–67.

Grossart, HP, Czub, G, Simon, M. 2006. Algae-bacteria interactions and their effects on aggregation and organic matter flux in the sea. *Environmental Microbiology* **8**: 1074–1084.

Guadayol, Ò, Marrasé, C, Peters, F, Berdalet, E, Roldán, C, Sabata, A. 2009a. Responses of coastal osmotrophic planktonic communities to simulated events of turbulence and nutrient load throughout a year. *Journal of Plankton Research* **31**: 583–600.

Guadayol, Ò, Peters, F, Marrasé, C, Gasol, JM, Roldán, C, Berdalet, E, Massana, R, Sabata, A. 2009b. Episodic meteorological and nutrient-load events as drivers of coastal planktonic ecosystem dynamics: A time-series analysis. *Marine Ecology Progress Series* **381**: 139–155.

Gutiérrez-Rodríguez, A, Latasa, M, Estrada, M, Vidal, M, Marrasé, C. 2010. Carbon fluxes through major phytoplankton groups during the spring bloom and post-bloom in the Northwestern Mediterranean Sea. *Deep Sea Research Part I: Oceanographic Research Papers* **57**: 486–500.

Hansen, HP, Grasshoff, K. 1983. Procedures for the automated determination of seawater constituents, in Grasshoff, K, Ehrhardt, M, Kremling, K eds., *Methods of seawater analysis.* 2nd ed. New York, NY: Verlag Chemie Weinhein: 362–379.

Harlay, J, Borges, AV, Van Der Zee, C, Delille, B, Godoi, RHM, Schiettecatte, LS, Roevros, N, Aerts, K, Lapernat, PE, Rebreanu, L, Groom, S, Daro, MH, Van Grieken, R, Chou, L. 2010. Biogeochemical study of a coccolithophore bloom in the northern Bay of Biscay (NE Atlantic Ocean) in June 2004. *Progress in Oceanography* **86**: 317–336.

Harlay, J, De Bodt, C, Engel, A, Jansen, S, d'Hoop, Q, Piontek, J, Van Oostende, N, Groom, S, Sabbe, K, Chou, L. 2009. Abundance and size distribution of transparent exopolymer particles (TEP) in a coccolithophorid bloom in the northern Bay of Biscay. *Deep Sea Research Part I: Oceanographic Research Papers* **56**: 1251–1265.

Hedges, JI. 2002. Why dissolved organics matter, in Hansell, DA, Carlson, CA eds., *Biogeochemistry of marine dissolved organic matter*. Orlando, FL: Academic Press: 1–33.

Hu, S, Smith, W. 1998. The effects of irradiance on nitrate uptake and dissolved organic nitrogen release by phytoplankton in the Ross Sea. *Continental Shelf Research* **18**: 971–990.

Iuculano, F, Duarte, CM, Marbà, N, Agustí, S. 2017a. Seagrass as major source of transparent exopolymer particles in the oligotrophic Mediterranean coast. *Biogeosciences Discussions* **14**: 5069–5075.

Iuculano, F, Mazuecos, IP, Reche, I, Agusti, S. 2017b. *Prochlorococcus* as a possible source for transparent exopolymer particles (TEP). *Frontiers in Microbiology* **8**: 709.

Jenkinson, IR, Seuront, L, Ding, H, Elias, F. 2018. Biological modification of mechanical properties of the sea surface microlayer, influencing waves, ripples, foam and air-sea fluxes. *Elementa: Science of the Anthropocene* **6**: 26.

Kirk, JTO. 1994. *Light and photosynthesis in aquatic ecosystems.* Canberra, Australia: Cambridge University Press.

Kuznetsova, M, Lee, C, Aller, J. 2005. Characterization of the proteinaceous matter in marine aerosols. *Marine Chemistry* **96**: 359–377.

Ling, S, Alldredge, AL. 2003. Does the marine copepod *Calanus pacificus* consume transparent exopolymer particles (TEP)? *Journal of Plankton Research* **25**: 507–515.

Long, RA, Azam, F. 1996. Abundant protein-containing particles in the sea. *Aquatic Microbial Ecology* **10**: 213–221.

Lucea, A, Duarte, CM, Agustí, S, Kennedy, H. 2005. Nutrient dynamics and ecosystem metabolism in the Bay of Blanes (NW Mediterranean). *Biogeochemistry* **73**: 303–323.

Lueck, S, Thurley, K, Thaben, PF, Westermark, PO. 2015. Rhythmic degradation explains and unifies circadian transcriptome and proteome data. *Cell Reports* **9**: 741–751.

Mari, X, Beauvais, S, Lemée, R, Pedrotti, M.L. 2001. Non-Redfield C: N ratio of transparent exopolymeric particles in the northwestern Mediterranean Sea. *Limnology and Oceanography* **46**: 1831–1836.

Mari, X, Burd, A. 1998. Seasonal size spectra of transparent exopolymeric particles (TEP) in a coastal sea and comparison with those predicted using coagulation theory. *Marine Ecology Progress Series* **171**: 63–76.

Mari, X, Passow, U, Migon, C, Burd, AB, Legendre, L. 2017. Transparent exopolymer particles: Effects on carbon cycling in the ocean. *Progress in Oceanography* **151**: 13–37.

Mari, X, Rochelle-Newall, E, Torréton, J-P, Pringault, O, Jouon, A. 2007. Water residence time: A regulatory factor of the DOM to POM transfer efficiency. *Limnology and Oceanography* **52**(2): 808–819.

Marty, J-C, Chiaverini, J, Pizay, M-D, Avril, B. 2002. Seasonal and interannual dynamics of nutrients and phytoplankton pigments in the western Mediterranean Sea at the DYFAMED time-series station

(1991–1999). *Deep Sea Research Part I* **49**: 1965–1985.

Menden-Deuer, S, Lessard, EJ. 2000. Carbon to volume relationships for dinoflagellates, diatoms, and other protist plankton. *Limnology and Oceanography* **45**: 569–579.

Norland, S. 1993. The relationship between biomass and volume of bacteria, in Kemp, PF, Sherr, EB, Cole, JJ eds., *Handbook of methods in aquatic microbial ecology*. Boca Raton, FL: Lewis Publishers: 303–307.

Ortega-Retuerta, E, Marrase, C, Munoz-Fernandez, A, Sala, MM, Simo, R, Gasol, J. M. 2018. Seasonal dynamics of transparent exopolymer particles (TEP) and their drivers in the coastal NW Mediterranean Sea. *Science of the Total Environment* **631–632**: 180–190.

Ortega-Retuerta, E, Mazuecos, IP, Reche, I, Gasol, JM, Álvarez-Salgado, XA, Álvarez, M, Montero, MF, Arístegui, J. 2019. Transparent exopolymer particle (TEP) distribution and in situ prokaryotic generation across the deep Mediterranean Sea and nearby North East Atlantic Ocean. *Progress in Oceanography* **173**: 180-191.

Ortega-Retuerta, E, Passow, U, Duarte, CM, Reche, I. 2009. Effects of ultraviolet B radiation on (not so) transparent exopolymer particles. *Biogeosciences* **6**: 3071–3080.

Parinos, C, Gogou, A, Krasakopoulou, E, Lagaria, A, Giannakourou, A, Karageorgis, AP, Psarra, S. 2017. Transparent exopolymer particles (TEP) in the NE Aegean Sea frontal area: Seasonal dynamics under the influence of Black Sea water. *Continental Shelf Research* **149**: 112–123.

Passow, U. 2002a. Production of transparent exopolymer particles (TEP) by phyto- and bacterioplankton. *Marine Ecology Progress Series* **236**: 1–12.

Passow, U. 2002b. Transparent exopolymer particles (TEP) in aquatic environments. *Progress in Oceanography* **55**: 287–333.

Passow, U. 2012. The abiotic formation of TEP under different ocean acidification scenarios. *Marine Chemistry* **128–129**: 72–80. Available at http://doi.org/10.1016/j.marchem.2011.10.004.

Passow, U, Alldredge, AL. 1994. Distribution, size and bacterial colonization of transparent exopolymer particles (TEP) in the ocean. *Marine Ecology Progress Series* **113**: 185–198.

Passow, U, Alldredge, AL. 1995. A dye-binding assay for the spectrophotometric measurement of transparent exopolymer particles (TEP). *Limnology and Oceanography* **40**: 1326–1335.

Piontek, J, Händel, N, Langer, G, Wohlers, J, Riebesell, U, Engel, A. 2009. Effects of rising temperature on the formation and microbial degradation of marine diatom aggregates. *Aquatic Microbial Ecology* **54**: 305–318.

Prieto, L, Ruiz, J, Echevarría, F, García, CM, Bartual, A, Gálvez, JA, Corzo, A, Macías, D. 2002. Scales and processes in the aggregation of diatom blooms: High time resolution and wide size range records in a mesocosm study. *Deep Sea Research I* **49**: 1233–1253.

Radic, T, Ivancic, I, Fuks, D, Radic, J. 2006. Marine bacterioplankton production of polysaccharidic and proteinaceous particles under different nutrient regimes. *FEMS Microbial Ecology* **58**: 333–342.

Radic, T, Kraus, R, Fuks, D, Radic, J, Pecar, O. 2005. Transparent exopolymeric particles' distribution in the northern Adriatic and their relation to microphytoplankton biomass and composition. *Science of the Total Environment* **353**: 151–161.

Ros, J, Gili, J-M. 2015. Four decades of research on the Medes Islands. *Contributions to Science* **11**: 75–83.

Sala, M, Peters, F, Gasol, JM, Pedrós-Alió, C, Marrasé, C, Vaqué, D. 2002. Seasonal and spatial variations in the nutrient limitation of bacterioplankton growth in the northwestern Mediterranean. *Aquatic Microbial Ecology* **27**: 47–56.

Sarmento, H, Romera-Castillo, C, Lindh, M, Pinhassi, J, Sala, MM, Gasol, JM, Marrase, C, Taylor, GT. 2013. Phytoplankton species-specific release of dissolved free amino acids and their selective consumption by bacteria. *Limnology and Oceanography* **58**: 1123–1135.

Schlitzer, R. 2017. Ocean data view. Available at http://odv.awi.de.

Scoullos, M, Plavšić, M, Karavoltsos, S, Sakellari, A. 2006. Partitioning and distribution of dissolved copper, cadmium and organic matter in Mediterranean marine coastal areas: The case of a mucilage event. *Estuarine, Coastal and Shelf Science* **67**: 484–490.

Shammi, M, Pan, X, Mostofa, KMG, Zhang, D, Liu, CQ. 2017. Photo-flocculation of microbial mat extracellular polymeric substances and their transformation into transparent exopolymer particles: Chemical and spectroscopic evidences. *Scientific Reports* **7**: 9074.

Simó, R, Vila-Costa, M, Alonso-Sáez, L, Cardelús, C, Guadayol, Ò, Vázquez-Domínguez, E, Gasol, JM. 2009. Annual DMSP contribution to S and C fluxes through phytoplankton and bacterioplankton in a NW Mediterranean coastal site. *Aquatic Microbial Ecology* **57**: 43–55.

Smetacek, V, Cloern, JE. 2008. Oceans. On phytoplankton trends. *Science* **319**: 1346–1348.

Smith, DC, Simon, M, Alldredge, AL, Azam, F. 1992. Intense hydrolytic enzyme-activity on marine aggregates and implications for rapid particle dissolution. *Nature* **359**: 139–142.

Stoderegger, K, Herndl, GJ. 1999. Production of exopolymer particles by marine bacterioplankton under contrasting turbulence conditions. *Marine Ecology Progress Series* **189**: 9–16.

Sun, C-C, Sperling, M, Engel, A. 2018. Effect of wind speed on the size distribution of biogenic gel particles in the sea surface microlayer: Insights from a wind wave channel experiment. *Biogeosciences* **15**: 3577–3589.

Suratman, S, Weston, K, Jickells, T, Chance, R, Bell, T. 2008. Dissolved organic matter release by an axenic culture of *Emiliania huxleyi*. *Journal of the Marine*

Biological Association of the United Kingdom **88(7)**: 1343–1346.

Taylor, JD, Cottingham, SD, Billinge, J, Cunliffe, M. 2014. Seasonal microbial community dynamics correlate with phytoplankton-derived polysaccharides in surface coastal waters. *Multidisciplinary Journal of Microbial Ecology* **8**: 245–248.

Taylor, JR, Ferrari, R. 2011. Shutdown of turbulent convection as a new criterion for the onset of spring phytoplankton blooms. *Limnology and Oceanography* **56**: 2293–2307.

Thornton, DCO. 2004. Formation of transparent exopolymeric particles (TEP) from macroalgal detritus. *Marine Ecology Progress Series* **282**: 1–12.

Thornton, DCO. 2018. Coomassie stainable particles (CSP): Protein-containing exopolymer particles in the ocean. *Frontiers in Marine Science* **5**: 206.

Thornton, DCO, Brooks, SD, Chen, J. 2016. Protein and carbohydrate exopolymer particles in the sea surface microlayer (SML). *Frontiers in Marine Science* **3**: 135.

Thornton, DCO, Chen, J. 2017. Exopolymer production as a function of cell permeability and death in a diatom (*Thalassiosira weissflogii*) and a cyanobacterium (*Synechococcus elongatus*). *Journal of Phycology* **53**: 245–260.

Trabelsi, L, Ben Ouada, H, Bacha, H, Ghoul, M. 2008. Combined effect of temperature and light intensity on growth and extracellular polymeric substance production by the cyanobacterium *Arthrospira platensis*. *Journal of Applied Phycology*, **21**: 405–412.

Utermöhl, H. 1958. Zur Vervollkommnung der quentitativen Phytoplankton-Methodik. *Mitteilungen der International Vereinigung fur heorestische und Angewandte Limnologie* **9**: 1–38.

von Jackowski, A, Grosse, J, Nöthig, E-M, Engel, A. 2020. Dynamics of organic matter and bacterial activity in the Fram Strait during summer and autumn. *Philosophical Transactions of the Royal Society* **378**: 20190366.

Wurl, O, Stolle, C, Van Thuoc, C, The Thu, P, Mari, X. 2016. Biofilm-like properties of the sea surface and predicted effects on air–sea CO_2 exchange. *Progress in Oceanography* **144**: 15–24.

Wurl, O, Wurl, E, Miller, L, Johnson, K, Vagle, S. 2011. Formation and global distribution of sea-surface microlayers. *Biogeosciences* **8**: 121–135.

Yamada, Y, Fukuda, H, Uchimiya, M, Motegi, C, Nishino, S, Kikuchi, T, Nagata, T. 2015. Localized accumulation and a shelf-basin gradient of particles in the Chukchi Sea and Canada Basin, western Arctic. *Journal of Geophysical Research: Oceans* **120**: 4638–4653.

Yentsch, CS, Menzel, DW. 1963. A method for the determination of phytoplankton chlorophyll and phaeophytin by fluorescence. *Deep Sea Research I* **10**: 221–231.

Zamanillo, M, Ortega-Retuerta, E, Nunes, S, Estrada, M, Sala, MM, Royer, S-J, López-Sandoval, DC, Emelianov, M, Vaqué, D, Marrasé, C, Simó, R. 2019a. Distribution of transparent exopolymer particles (TEP) in distinct regions of the Southern Ocean. *Science of the Total Environment* **691**: 736–748.

Zamanillo, M, Ortega-Retuerta, E, Nunes, S, Rodríguez-Ros, P, Dall'Osto, M, Estrada, M, Sala, MM, Simó, R. 2019b. Main drivers of transparent exopolymer particle distribution across the surface Atlantic Ocean. *Biogeosciences* **16**: 733–749.

Zancker, B, Bracher, A, Rottgers, R, Engel, A. 2017. Variations of the organic matter composition in the sea surface microlayer: A comparison between open ocean, coastal, and upwelling sites off the Peruvian coast. *Frontiers in Microbiology* **8**: 2369.

How to cite this article: Zamanillo, M, Ortega-Retuerta, E, Cisternas-Novoa, C, Marrasé, C, Pelejero, C, Pascual, J, Gasol, JM, Engel, A, Simó, R. 2021. Uncoupled seasonal variability of transparent exopolymer and Coomassie stainable particles in coastal Mediterranean waters: Insights into sources and driving mechanisms. *Elementa: Science of the Anthropocene* 9(1). DOI: https://doi.org/10.1525/elementa.2020.00165

Domain Editor-in-Chief: Jody W. Deming, University of Washington, Seattle, WA, USA

Associate Editor: Laurenz Thomsen, School of Engineering and Science, Department of Earth and Space Sciences, Jacobs University Bremen, Bremen, Germany

Knowledge Domain: Ocean Science

Published: December 3, 2021 **Accepted:** August 7, 2021 **Submitted:** November 4, 2020